

## Characterizing and Modeling Mechanical Properties of Nanocomposites- Review and Evaluation

Hurang Hu<sup>a\*</sup>, Landon Onyebueke<sup>a</sup>, Ayo Abatan<sup>b</sup>

<sup>a</sup>Department of Mechanical and Manufacturing Engineering, Tennessee State University,  
Nashville, TN 37209, USA

<sup>b</sup>Department of Engineering Technology, Miami University, Hamilton, OH 45011, USA

\*Corresponding Author: [hhu@tnstate.edu](mailto:hhu@tnstate.edu)

### **ABSTRACT**

*This paper presents a critical review of the current work of experiment, theory of micro-nano-mechanics, and numerical analysis on characterizing mechanical properties of nanocomposites. First, the classifications of nanomaterials are presented. Then nanoindentation testing and the corresponding finite element modeling are discussed, followed by analytical modeling stiffness of nanocomposites. The analytical models discussed include Voigt and Reuss bounds, Hashin and Shtrikman bounds, Halpin–Tsai model, Cox model, and various Mori and Tanaka models. These micromechanics models predict stiffness of nanocomposites with both aligned and randomly oriented fibers. The emphasis is on numerical modeling includes molecular dynamics modeling and finite element modeling. Three different approaches are discussed in finite element modeling, i.e. multiscale representative volume element (RVE) modeling, unit cell modeling, and object-oriented modeling. Finally, the mechanism of nanocomposite mechanical property enhancement and the ways to improve stiffness and fracture toughness for nanocomposites are discussed.*

**Key words:** *Nanocomposites; Mechanical properties; Multiscale modeling; Finite element analysis (FEA); Object-oriented modeling.*

### **1. INTRODUCTION**

Nanoscience and nanotechnology refer to the understanding and control of matter at the atomic, molecular or macromolecular levels, at the length scale of approximately 1 to 100

nanometers, where unique phenomena enable novel applications. Nanotechnologies are the design, characterization, production and application of structures, devices and systems by controlling shape and size at nanometer scale. According to Braun et al. [1], from 1980s, the growth of research papers dealing with the prefix called 'nano' is exponential. Among all the work, characterizing and modeling mechanical properties of nanocomposites is one of the most important subjects.

Nanocomposites are composite materials in which the matrix material is reinforced by one or more separate nanomaterials in order to improve performance properties. The most common materials used as matrix in nanocomposites are polymers (e.g. epoxy, nylon, polyepoxide, polyetherimide), ceramics (e.g. alumina, glass, porcelain), and metals (e.g. iron, titanium, magnesium).

Nanomaterials are generally considered as the materials that have a characteristic dimension (e.g. grain size, diameter of cylindrical cross-section, layer thickness) smaller than 100 nm. Nanomaterials can be metallic, polymeric, ceramic, electronic, or composite. Nanomaterials are classified into three categories depending on their geometry, as shown in Fig. 1 [2,3]:

1. Nanoparticles: When the three dimensions of particulates are in the order of nanometers, they are referred as equi-axed (isodimensional) nanoparticles or nanogranules or nanocrystals.

2. Nanotubes: When two dimensions are in the nanometer scale and the third is larger, forming an elongated structure, they are generally referred as 'nanotubes' or nanofibers/whiskers/nanorods.

3. Nanolayers: The particulates which are characterized by only one dimension in nanometer scale are nanolayers/nanoclays/nanosheets/nanoplatelets. These particulate is present in the form of sheets of one to a few nanometer thick to hundreds to thousands nanometers long.

The nanomaterials can also be distinguished in three types as natural, incidental, and engineered nanomaterials depending on their pathway [4]. Natural nanomaterials, which are formed through natural processes, occur in the environment (e.g. volcanic dust, lunar dust, magneto-tactic bacteria, minerals, etc.). Incidental nanomaterials occur as the result of man made industrial processes (e.g. coal combustion, welding fumes, etc.). Engineered nanomaterials are produced either by lithographically etching of a large sample to obtained nanoparticles, or by assembling smaller subunits through crystal growth or chemical synthesis to grow nanomaterials of the desired size and configuration. Engineered nanomaterials most often have regular shapes, such as tubes, spheres, rings, etc. U.S. Environmental Protection Agency divides engineered nanomaterials into four types. They are carbon-based materials (nanotubes, fullerenes), metal-based materials (including both metal oxides and quantum dots), dendrimers (nanosized

polymers built from branched units of unspecified chemistry), and composites (including nanoclays).

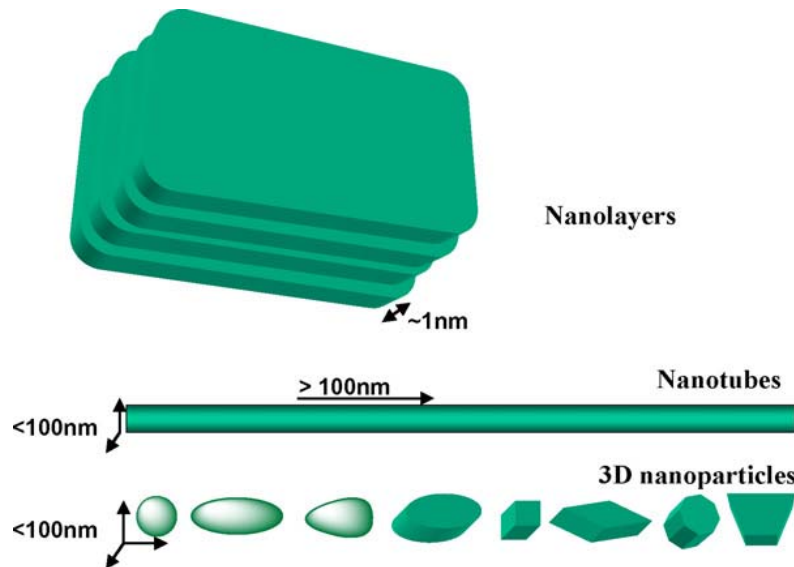


Figure 1. Various types of nanoscale materials [4].

Comparing to the conventional micro-composites, nanocomposites greatly improve the physical and mechanical properties. The nanoscale reinforcements over traditional fillers have the following advantages [5]:

1. Low-percolation threshold ( $\sim 0.1\text{--}2$  vol.%).
2. Large number density of particles per particle volume ( $10^6\text{--}10^8$  particles/ $\mu\text{m}^3$ ).
3. Extensive interfacial area per volume of particles ( $10^3\text{--}10^4$   $\text{m}^2/\text{ml}$ ).
4. Short distances between particles (10–50nm at  $\sim 1\text{--}8$  vol.%).

Although any kind of material can be produced to appear in a nanoscaled shape and size, carbon nanotubes and nanoplatelets as shown in Fig. 2 are the two kinds of nanoparticles that gained the most attention [6].

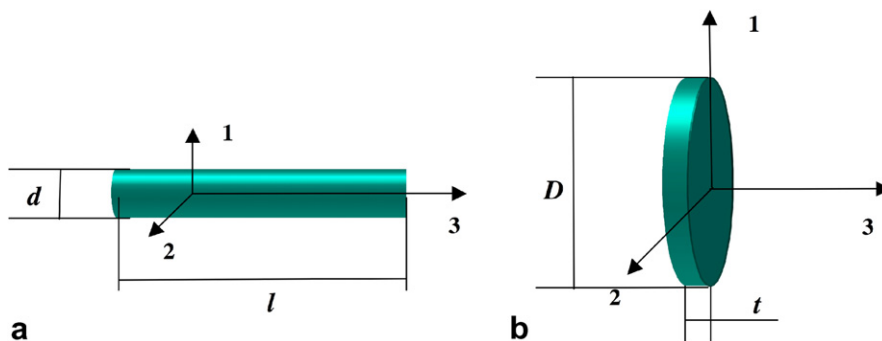


Figure 2. Schematic of (a) nanotube and (b) nanoplatelet [6].

This paper presents a thorough review of characterizing and modeling mechanical properties of nanocomposites. The critical review covers the current work on the experiment, theory, and numerical analysis in this area. Nanoindentation testing and the finite element modeling are discussed, followed by analytical modeling stiffness of nanocomposites. The numerical modeling includes molecular dynamics modeling and finite element modeling. Three different approaches are discussed in finite element modeling, i.e. multiscale representative volume element (RVE) modeling, unit cell modeling, and object-oriented modeling. Finally, the mechanism of nanocomposites mechanical property enhancement is explored, and the ways to improve their stiffness and fracture toughness are discussed.

## 2. CHARACTERIZING AND MODELING OF NANOCOMPOSITES

### 2.1 Nanoindentation Tests and Computing Simulations

There are different ways to experimentally characterize nanocomposites. For example, tensile and flexural tests (mostly conducted on Instron machines), impact tests (conducted on pendulum impact testing machine) [7-11], and micro-compression tests [12,13]. Nanoindentation test is one of the most effective and widely used methods to measure the mechanical properties of materials. This technique uses the same principle as microindentation, but with much smaller probe and loads, so as to produce indentations from less than a hundred nanometers to a few micrometers in size. During the past dozen years or so, it has been widely used in measuring the mechanical properties of various nanocomposites [14-25] and human enamel and dentin [26-38].

Hardness (H) and elastic modulus (E) are calculated from the load-displacement curve obtained from a nanoindentation test. A typical load-displacement curve is shown in Fig. 3. As the indenter penetrates into the specimen, the loading curve climbs up. At some point, the maximum load  $P_{\max}$  is reached, and then followed by the unloading. If the material is perfectly elastic and has no hysteresis, the loading curve and the unloading curve will be identical.  $h_{\max}$  gives a measure of the total maximum deformation, while  $h_f$  represents the maximum permanent (plastic) deformation (final penetration depth).

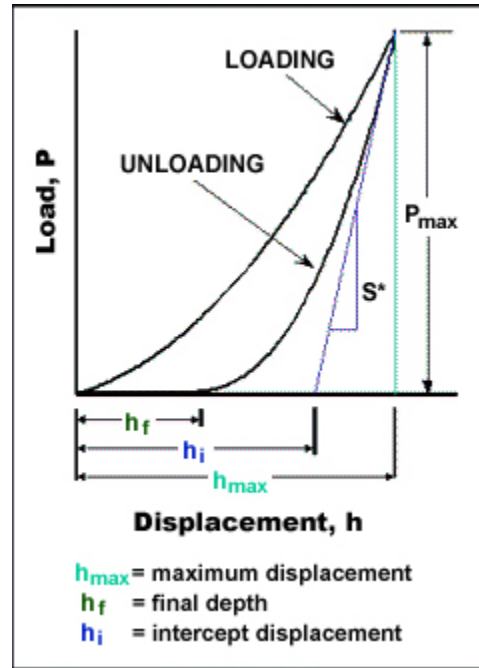


Figure 3. Typical load-displacement curve of the nanoindentation test.

The most commonly used method to obtain the hardness and the elastic modulus of a material by nanoindentation is the Oliver-Pharr method [25]. According to this method, the nanoindentation hardness as a function of the final penetration depth of indent can be determined by:

$$H = \frac{P_{\max}}{A} \quad (2.1)$$

where  $P_{\max}$  is the maximum applied load measured at the maximum depth of penetration ( $h_{\max}$ ),  $A$  is the projected contact area between the indenter and the specimen. For a spherical indenter,  $A = 2\pi R h_f$  (where  $R$  is the radius of the indenter), whereas for a pyramidal (Berkovich or Vickers) indenter,  $A$  can be expressed as a function of  $h_f$  as

$$A = 24.504h_f^2 + C_1h_f + C_2h_f^{1/2} + C_3h_f^{1/4} + \dots + C_8h_f^{1/128} \quad (2.2)$$

where  $C_1$  to  $C_8$  are constants and can be determined by standard calibration procedure. The final penetration depth,  $h_f$ , can be determined from the following expression:

$$h_f = h_{\max} - \varepsilon \frac{P_{\max}}{S^*} \quad (2.3)$$

where  $\varepsilon$  is a geometric constant,  $\varepsilon=0.75$  for a pyramidal indenter, and  $\varepsilon=0.72$  for a conical indenter.  $S^*$  is the contact stiffness which can be determined as the slope of the unloading curve at the maximum loading point, i.e.

$$S^* = \left( \frac{dP}{dh} \right)_{h=h_{\max}} \quad (2.4)$$

The reduced elastic modulus  $E_r$  is given by

$$E_r = \frac{S^*}{2\beta} \sqrt{\frac{\pi}{A}} \quad (2.5)$$

where  $\beta$  is a constant that depends on the geometry of the indenter. For both a Berkovich and a Vicker's indenter,  $\beta=1.034$ , whereas for both a conical and a spherical indenter,  $\beta=1$ . The specimen elastic modulus ( $E_s$ ) can then be calculated as:

$$\frac{1}{E_r} = \frac{1-\nu_s^2}{E_s} + \frac{1-\nu_i^2}{E_i} \quad (2.6)$$

Where  $E_{i,s}$  and  $\nu_{i,s}$  are the elastic modulus and Poisson's ratio, respectively, for the indenter and the specimen. For a diamond indenter,  $E_i$  is 1140 GPa and  $\nu_i$  is 0.07. The contact stiffness,  $S^*$ , can be derived from the unloading curve which simply obeys the following power law

$$P = B(h - h_f)^n \quad (2.7)$$

where  $B$  and  $n$  are empirical constants that can be determined by fitting the experimentally measured pairs of data ( $P, h$ ) during unloading. Thus the contact stiffness can be expressed as

$$S^* = \left( \frac{dP}{dh} \right)_{h=h_{\max}} = Bn(h_{\max} - h_f)^{n-1} \quad (2.8)$$

Therefore, the specimen's hardness  $H$  and elastic modulus  $E_s$  will be obtained from this set of equations.

Indentation is a highly nonlinear problem. It involves large plastic deformation, material nonlinearity, and contact. In order to better understand and characterize the mechanical properties and to provide guidelines for proper design of experiments, finite element method is often used to simulate the nanoindentation tests [14, 15, 18, 38-51]. It is also noted that the primary mechanical properties extracted from a nanoindentation test are the hardness and the elastic modulus. Finite element simulation could be employed to get other properties, such as yield stress and hardening [38, 52-58]. Fig. 4(a) shows the geometry of indentation of a cylindrical specimen with a conical indenter, and 4(b) shows the Mises stress contour from the finite element analysis [15]. Note that the finite element meshes are the two-dimensional (axisymmetric) elements. Fig. 5 shows a three-dimensional nanoindentation finite element mesh system [18]. Note that because of symmetry, only half of the specimen volume was modeled.

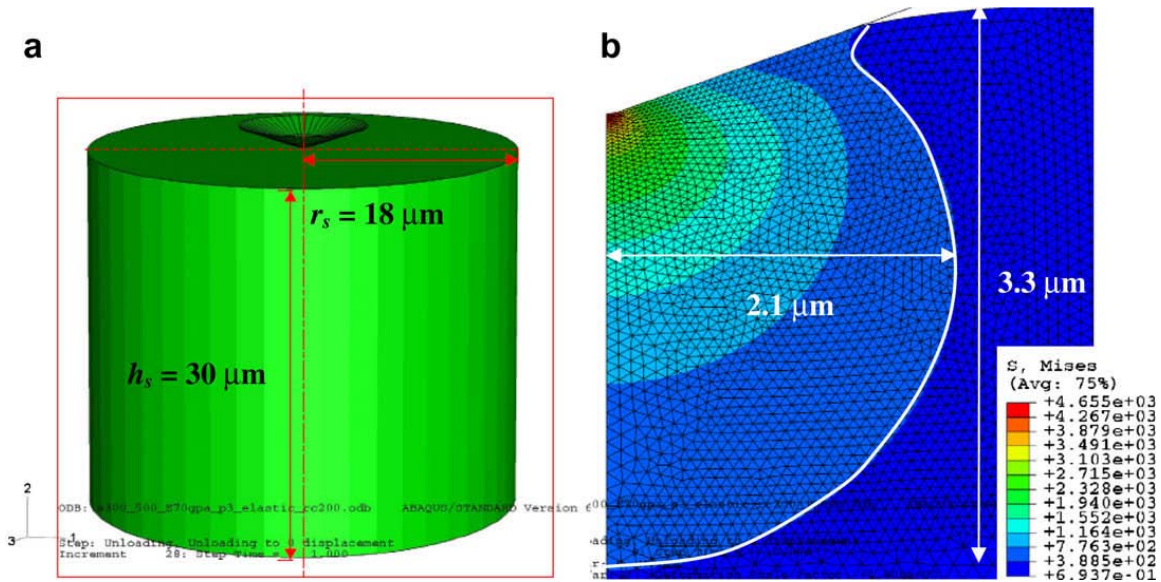


Figure 4. (a) Geometry of indentation of a cylindrical specimen with a conical indenter. (b) The Mises equivalent stress field in the specimen during indentation at  $h_{\text{max}} = 600 \text{ nm}$ . (The stress values must be multiplied by  $10^7$  to respect the scale of the problem) [15].

## 2.2 Analytical Modeling Stiffness of Nanocomposites

It is well known that composite materials have advantages over traditional materials. Nanocomposites, where nano-sized reinforcements (fillers) are dispersed in the base material (matrix), offer a novel class of composites with superior properties and added functionalities [59-62]. Although the applicability of continuum mechanics (including micro mechanics) to nanocomposites has been subjected to debate [59,63], many recent works directly applying continuum mechanics to nanostructures and nanomaterials have reported meaningful results and elucidated many issues [64-73]. Thus, mechanics-based formulas for predicting the mechanical properties will be reviewed.

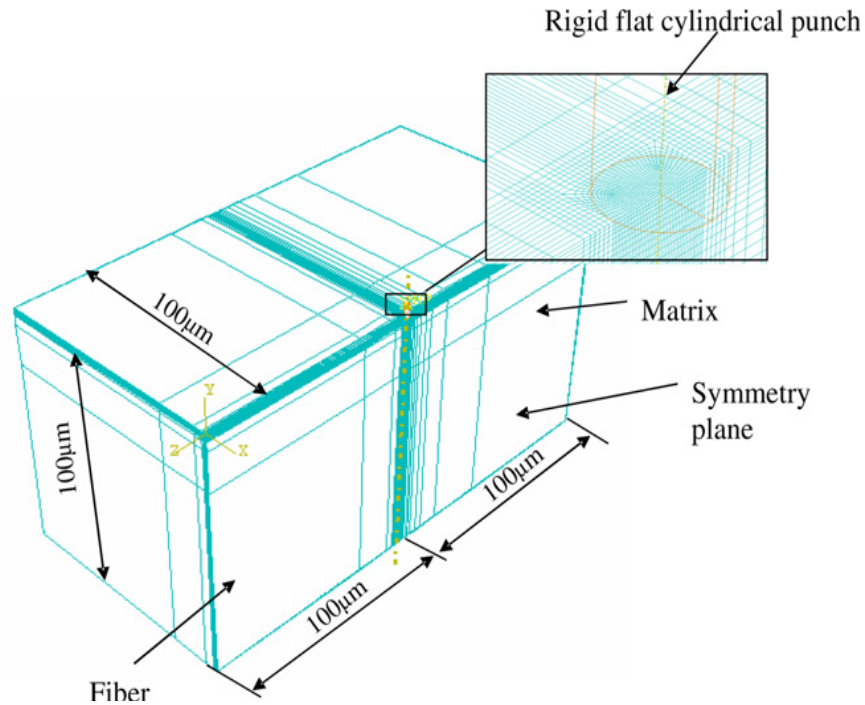


Figure 5. Illustration of a three dimensional nanoindentation finite element model [18].

In nanocomposites, there are typically three kinds of fillers. They are cylinder-like nanofibers (nanotubes), flake-like (disk-like) platelets (nanolayers, nanoclays), and spheroid-like particulates, refer to Figs. 1 and 2. For the fiber-reinforced nanocomposites, there are two cases depending on the orientation of the fibers, i.e. aligned fibers and randomly oriented fibers, see Fig. 6 below.

The popular micromechanical models for prediction of modulus of elasticity are summarized and discussed in the following:

### 2.2.1 Voigt upper bound and Reuss lower bound (V-R model)

Assumed aligned fibers, and fibers and matrix are subjected to the same uniform strain in the fiber direction, Voigt [74] got the effective modulus in the fiber direction as:

$$E_L = \phi E_f + (1 - \phi) E_m \quad (2.9)$$

Reuss [75] applied the same uniform stress on the fiber and matrix in the transverse direction (normal to the fiber direction), and got the effective modulus in the transverse direction as:

$$\frac{1}{E_T} = \frac{\phi}{E_f} + \frac{1 - \phi}{E_m} \quad (2.10)$$

where  $\phi$  is the volume fraction of fiber in the two-phase composite system, and subscripts “f” and “m” respectively refer to the fiber and matrix, whereas the subscripts “L” and “T” refer to

the longitudinal and transverse directions, respectively. Equation (2.9) is the parallel coupling formula, and it is also called the “rule of mixtures”, whereas (2.10) is the series coupling formula, and it is also called the “inverse rule of mixtures”.

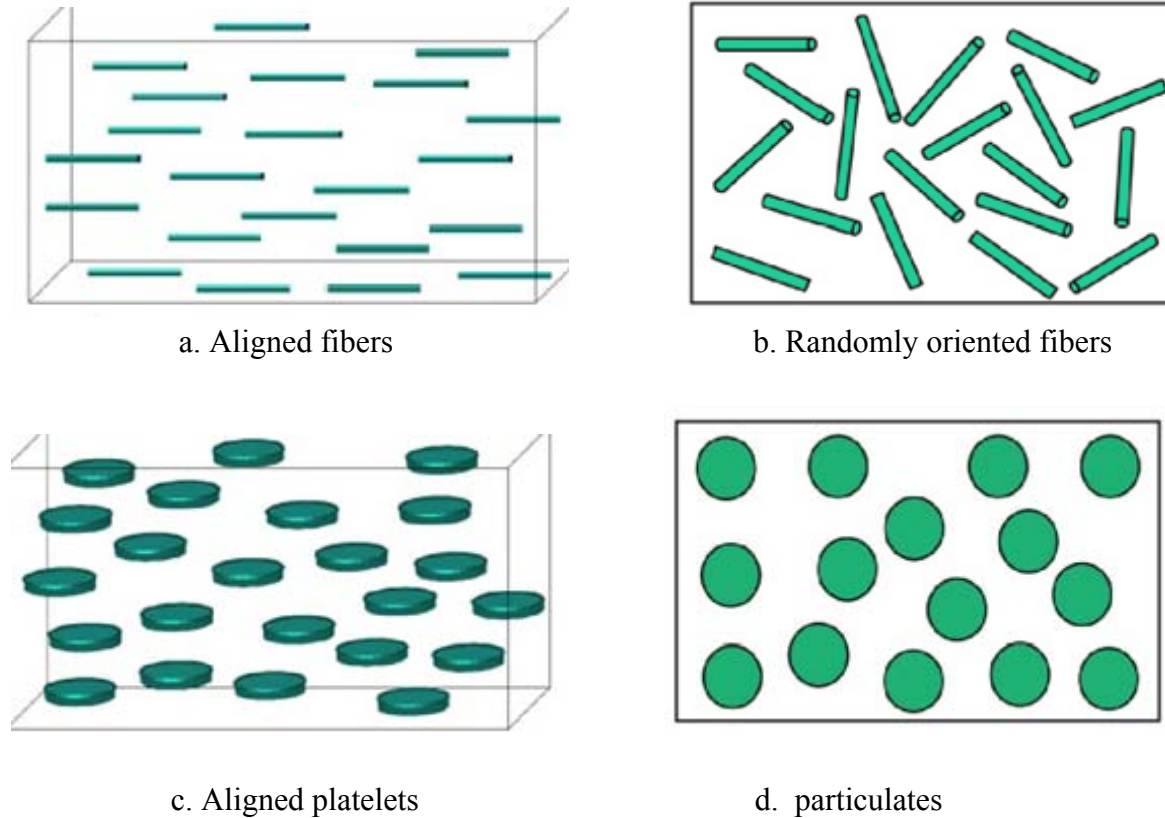


Figure 6. Schematics of nanocomposites: (a) with aligned fibers; (b) with randomly oriented fibers; (c) with aligned platelets; and (d) with randomly oriented particulates [6].

Equations (2.9) and (2.10) can be extended to any two-phase composites regardless the shape of the filler, and  $E_L$  and  $E_T$  represent the upper and lower bounds of the modulus of the composite, respectively. Note that in these formulas, only three parameters are involved, i.e. modulus of the fiber and the matrix, and the fiber volume fraction.

### 2.2.2 Hashin and Shtrikman upper and lower bounds (H-S model)

Hashin and Shtrikman [76,77] assumed macroscopical isotropy and quasi-homogeneity of the composite where the shape of the filler is not a limiting factor, and estimated the upper and lower bounds of the composite based on variational principles of elasticity. Depending on whether the stiffness of the matrix is more or less than that of the filler, the upper and lower bounds of the

bulk moduli,  $K_{upper}$  and  $K_{lower}$ , and shear moduli,  $G_{upper}$  and  $G_{lower}$ , of the composite are given as:

$$K_{upper} = K_f + (1 - \phi) \left[ \frac{1}{K_m - K_f} + \frac{3\phi}{3K_f + 4G_f} \right]^{-1} \quad (2.11)$$

$$K_{lower} = K_m + \phi \left[ \frac{1}{K_f - K_m} + \frac{3(1 - \phi)}{3K_m + 4G_m} \right]^{-1} \quad (2.12)$$

$$G_{upper} = G_f + (1 - \phi) \left[ \frac{1}{G_m - G_f} + \frac{6\phi(K_f + 2G_f)}{5G_f(3K_f + 4G_f)} \right]^{-1} \quad (2.13)$$

$$G_{lower} = G_m + \phi \left[ \frac{1}{G_f - G_m} + \frac{6(1 - \phi)(K_m + 2G_m)}{5G_m(3K_m + 4G_m)} \right]^{-1} \quad (2.14)$$

where the subscripts “f” and “m” refer to the filler (fiber) and matrix, respectively. The upper and lower bounds of the elastic modulus can then be calculated using the following relation:

$$E = \frac{9K}{1 + 3K/G} \quad (2.15)$$

Similar to Voigt and Reuss models, H-S model only involves three parameters.

### 2.2.3 Halpin-Tsai model (H-T model)

For aligned fiber-reinforced composite materials, Halpin and Tsai [78-81] developed the equations for prediction of elastic constants based on the work of Hermans [82] and Hill [83]. The H-T model is a semi-empirical model, and the longitudinal and transverse moduli are given by:

$$E_L = \frac{1 + 2(l/d)\phi\eta_L}{1 - \phi\eta_L} E_m \quad (2.16)$$

$$E_T = \frac{1 + 2\phi\eta_T}{1 - \phi\eta_T} E_m \quad (2.17)$$

where  $l$  and  $d$  are the length and diameter of the fiber, and  $\eta_L$  and  $\eta_T$  take the following expressions:

$$\eta_L = \frac{E_f - E_m}{E_f + 2(l/d)E_m} \quad (2.18)$$

$$\eta_T = \frac{E_f - E_m}{E_f + 2E_m} \quad (2.19)$$

For aligned nanoplatelets as shown in Fig. 6 (c), equations (2.16) to (2.19) may still be used by replacing  $(l/d)$  with  $(D/t)$ , where  $D$  and  $t$  are respectively the diameter and thickness of the platelet (refer to Fig. 2).

H-T model takes the consideration of the fiber geometry, and has five independent parameters.

### 2.2.4 Hui-Shia model (H-S model)

Mori and Tanaka [84] developed analytical expressions for elastic constants based on the equivalent inclusion model of Eshelby [85]. Taya and Mura [86] and Taya and Chou [87] used Mori-Tanaka approach to predict the longitudinal modulus of fiber-reinforced composites, Weng [88] and Tandon and Weng [89] further developed equations for the complete set of elastic constants of composite materials with aligned spheroidal isotropic inclusions. Based upon the results of Tandon and Weng [89], Hui and Shia [90] and Shia et al. [91] derived simplified formulas for predicting the overall moduli of composites with aligned reinforcements with emphases on fiber-like and flake-like reinforcements, and found that their theoretical predictions agree well with experimental results. The H-S model presents the Young's modulus as follows:

$$E_L = E_m \left[ 1 - \frac{\phi}{\xi} \right]^{-1} \quad (2.20)$$

$$E_T = E_m \left[ 1 - \frac{\phi}{4} \left( \frac{1}{\xi} + \frac{3}{\xi + \Lambda} \right) \right]^{-1} \quad (2.21)$$

where

$$\xi = \phi + \frac{E_m}{E_f - E_m} + 3(1 - \phi) \left[ \frac{(1 - g)\alpha^2 - g/2}{\alpha^2 - 1} \right] \quad (2.22)$$

$$\Lambda = (1 - \phi) \left[ \frac{3(\alpha^2 + 0.25)g - 2\alpha^2}{\alpha^2 - 1} \right] \quad (2.23)$$

$$g = \begin{cases} \frac{\alpha}{(\alpha^2 - 1)^{3/2}} [\alpha\sqrt{\alpha^2 - 1} - \cosh^{-1} \alpha] & \alpha \geq 1 \\ \frac{\alpha}{(1 - \alpha^2)^{3/2}} [-\alpha\sqrt{1 - \alpha^2} + \cos^{-1} \alpha] & \alpha \leq 1 \end{cases} \quad (2.24)$$

and  $\alpha$  is the aspect ratio of the filler, defined as the ratio of the filler's longitudinal (with Young's modulus  $E_L$ ) length to its transverse (with Young's modulus  $E_T$ ) length. For example, refer to Fig. 2,  $\alpha = l/d$  for nanotube,  $\alpha = t/D$  for nanoplatelet, and  $E_L$  will be along axis 3, and  $E_T$  will be along axis 1 (or 2).

### 2.2.5 Wang-Pyrz model (W-P model)

For a composite material composed of an isotropic matrix and randomly oriented transversely isotropic spheroids, Qiu and Weng [92] and Chen et al. [93] gave the formulas for the overall bulk and shear moduli using the Mori-Tanaka method. These formulas are expressed in terms of

the Eshelby tensor [85], thus are not final. Wang and Pyrz [94] further gave the closed and concise formulas for the overall bulk modulus and shear modulus as follows:

$$K = K_m + K_m \frac{\phi\phi}{1 - \phi(1 - \alpha)} \quad (2.25)$$

$$\mu = \mu_m + \mu_m \frac{\phi\psi}{1 - \phi(1 - \beta)} \quad (2.26)$$

The expressions for  $\phi$ ,  $\psi$ ,  $\alpha$  and  $\beta$  are given in the Appendix.

Note that W-P model is based on the Mori-Tanaka approach, and deals with the composite materials reinforced with randomly oriented and transversely isotropic spheroids. By varying the aspect ratio, the oblate spheroids can be approximate to platelets, and the prolate spheroids can be approximate to fibers.

### 2.2.6 Cox model (Shear lag model)

Shear lag model was the first micro-mechanics model for fiber-reinforced composites. Cox [95] analyzed a single fiber of length  $l$  and radius  $r_f$ , which is encased in a concentric cylindrical shell of matrix having radius  $R$ . He derived the longitudinal modulus as

$$E_L = \eta_L \phi E_f + (1 - \phi) E_m \quad (2.27)$$

where  $\eta_L$  is a length-dependent efficiency factor,

$$\eta_L = 1 - \frac{\tanh(\beta l / 2)}{\beta l / 2} \quad (2.28)$$

with

$$\beta^2 = \frac{4\mu_m}{r_f^2 E_f \ln(K_R / \phi)} \quad (2.29)$$

$K_R$  is a constant that depends on the fiber packing arrangements. For some typical fiber packing arrangements, the values of  $K_R$  are given in Table 1 [96].

Table 1. Values for  $K_R$  in Eq. (2.29)

FIBER PACKING	$K_R$
Cox	$2\pi / \sqrt{3} = 3.628$
Composite cylinders	1.000
Hexagonal	$\pi / 2\sqrt{3} = 0.907$
Square	$\pi / 4 = 0.785$

It is well known that the orientation of the dispersed phase has a dramatic effect on the composite modulus. It is apparent from their geometry that flake-like platelets can provide equal

reinforcement in two directions, if appropriately oriented, while fibers provide primary reinforcement in one direction. If the longitudinal modulus  $E_L$  and the transverse modulus  $E_T$  are known, then the effective modulus of the composite with randomly oriented fibers and platelets in all three orthogonal directions are given by [97]:

$$E_{3D}^{fiber} = 0.184E_L + 0.816E_T \quad (2.30)$$

$$E_{3D}^{platelet} = 0.49E_L + 0.51E_T \quad (2.31)$$

### 2.3 Molecular Dynamics Simulation

In modeling mechanical properties of nanocomposites, there are two main approaches: one is molecular dynamics simulation using direct methods, and the other is finite element simulation using “continuum” methods. Molecular dynamics simulation is a technique that allows one to determine the physical and mechanical properties of materials in nanoscale through solving Newton’s equations of motion with the atoms interacting through assumed interatomic potentials [98, 99]. It generates information such as atomic positions, velocities and forces from which some macroscopic properties can be derived by means of statistical mechanics. Molecular dynamics simulation usually consists of three constituents: (1) a set of initial conditions (e.g., initial positions and velocities of all particles in the system); (2) the interaction potentials to represent the forces among all the particles; (3) the evolution of the system in time by numerically solving a set of classical Newtonian equations of motion for all particles in the system [100]. In 1997, Cornwell et al. used molecular dynamics to predict the elastic properties of single-walled carbon nanotubes [101]. In recent years, molecular dynamics simulation has been extensively used in predicting mechanical properties of carbon nanotubes and nanotubes reinforced composites [102-109], graphite/epoxy nanocomposites [110-112], and other nanocomposites [113-119].

Molecular dynamics simulation involves the proper selection of interaction potentials, numerical integration, periodic boundary conditions, and the controls of pressure and temperature to mimic physically meaningful thermodynamic ensembles. The interaction potentials together with their parameters form a force field which describes in detail how the particles in a system interact with each other. Such a force field may be obtained by quantum method, empirical method or quantum-empirical method. The criteria for selecting a force field include the accuracy, transferability and computational speed. The total potential energy  $U$  may consist of a number of bonded and non-bonded interaction terms:

$$U = \sum U_{bond} + \sum U_{angle} + \sum U_{torsion} + \sum U_{inversion} + \sum U_{non-bonded} \quad (2.32)$$

The first four terms represent bonded interactions, i.e., bond-stretching between two bonded atoms, angle-bending by three neighboring atoms, angle variation between two planes formed by four neighboring atoms, and angle variation of two planes formed by four atoms where one atom

is bonded to other three, as shown in Fig. 7 [120]. The last term represents non-bonded interactions between two atoms. It usually includes van der Waals and electrostatic interactions.

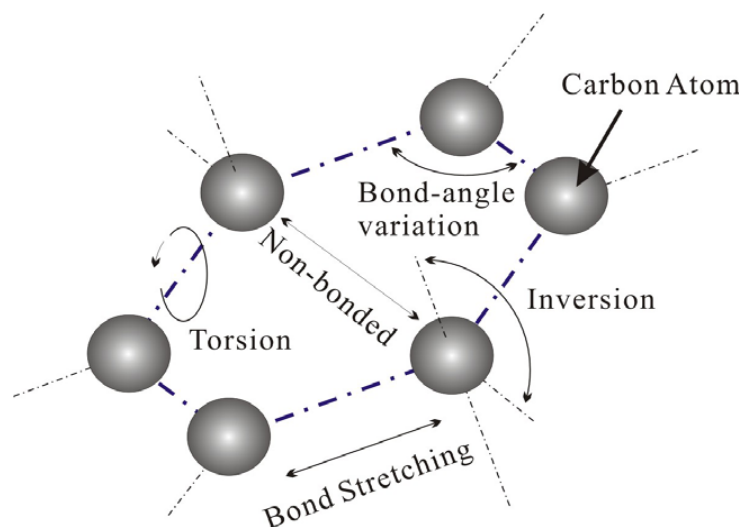


Figure 7. Bond structures and corresponding energy terms of a graphene cell [120].

Molecular dynamics simulations can be performed in different ensembles, such as grand canonical ( $\mu VT$ ), microcanonical (NVE), canonical (NVT) and isothermal–isobaric (NPT). The constant temperature and pressure can be controlled by adding an appropriate thermostat (e.g., Berendsen, Nose, Nose–Hoover and Nose–Poincare) and barostat (e.g., Andersen, Hoover and Berendsen), respectively. The software packages available for molecular dynamics simulations include DL-POLY developed by Daresbury Laboratory [121, 122], LAMMPS developed by Sandia National Laboratories [123], and TINKER developed by University of Washington [124].

To demonstrate how to use molecular dynamics simulation to evaluate the mechanical properties of nanocomposites, the work by Adnan et al. [125] using molecular dynamics simulation to investigate the effect of filler size on elastic properties of polymer nanocomposites will be presented below. Adnan et al. constructed the nanocomposite by reinforcing amorphous polyethylene (PE) matrix with nano sized buckminster fullerene bucky-ball. Three types of bucky-balls,  $C_{60}$ ,  $C_{180}$ , and  $C_{320}$  (subscripts denote number of carbon atoms) with three different diameters (0.7, 1.2 and 1.7 nm, respectively) were utilized to incorporate size effect in the nanocomposites. The PE matrix was represented by united atom (UA)- $CH_2$ - units. All bucky-balls were infused in matrix by approximately 4.5 vol%. Once the molecular structures were developed, the corresponding molecular mechanics force fields were defined. The PE chains were described by appropriate bond stretching, angle bending and dihedral potentials between - $CH_2$ - units. The non-bonded van der Waals interactions within or between PE chains were modeled using lennard-Jones (LJ) potential [126, 127]. The functional form and parameters of the force field are shown in Table 2.

Table 2. Functional form and parameters for the force field [125]

Interaction	Potential	Functional form	Parameters
Bond	Harmonic	$U(r) = \frac{1}{2}k_r(r - r_0)^2$	$k_r = 700$ kcal/mol $r_0 = 1.53 \text{ \AA}$
Angle	Harmonic cosine	$U(\theta) = \frac{1}{2}k_\theta[\cos(\theta) - \cos(\theta_0)]^2$	$k_\theta = 112.5$ kcal/mol $\theta_0 = 109.471^\circ$
Dihedral	Cosine	$U(\phi) = \frac{1}{2}k_\phi[1 + \cos(m\phi)]^2$	$k_\phi = 1.00$ kcal/mol, $m=3$
Non-bonded	Lennard-Jones	$U(r) = \begin{cases} 4\varepsilon \left[ \left(\frac{\sigma}{r}\right)^{12} - \left(\frac{\sigma}{r}\right)^6 \right] & r < r_{cut} \\ 0 & r \geq r_{cut} \end{cases}$	<b>PE-PE:</b> $\varepsilon = 0.113266$ kcal/mol $\sigma = 4.28 \text{ \AA}$ <b>PE-Bucky:</b> $\varepsilon = 0.107290$ kcal/mol $\sigma = 3.825 \text{ \AA}$ $r_{cut} = 10.7 \text{ \AA}$

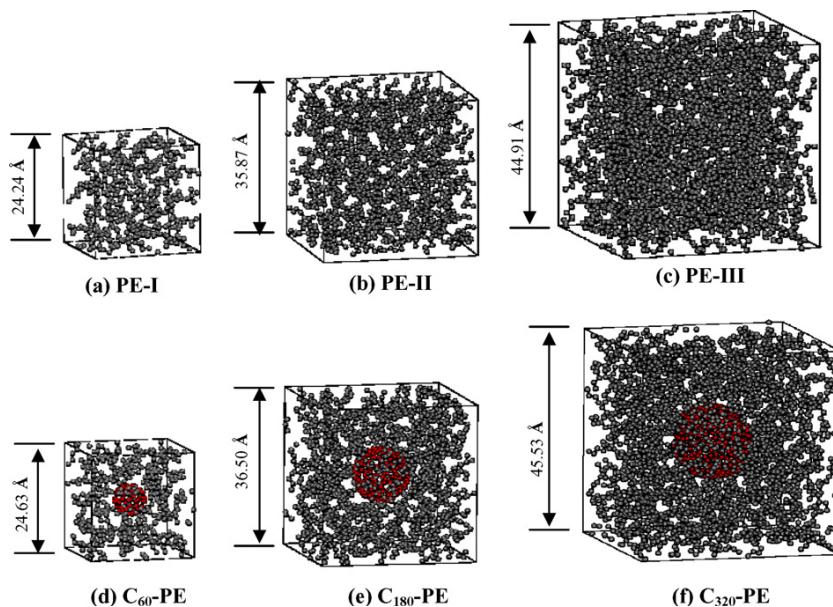


Figure 8. Cells of different neat and nanocomposites model used for simulation [125].

Fig. 8 shows the cells of different neat and nanocomposites model used for simulation. Periodic boundary conditions were employed to replicate the unit cells in three dimensions. Software package DL\_PLOY (version 2.14) was used in the simulation. All the calculations were carried out at a temperature of 300<sup>0</sup>K with 0.5 fs time steps. Two major steps of simulation for both neat polymer and nanocomposites were performed. In the first step, the equilibrium state of the molecular model was obtained, and then the model was subjected to different strain fields and re-equilibrated. Adnan et al. applied a uniform strain field (0.5%) to the periodic cells of both neat polymer and nanocomposites. For the cases of hydrostatic tension and hydrostatic compression, they evaluated the bulk modulus  $K$ , and their results were shown in Table 3.

Table 3. Evaluation of bulk modulus  $K$  for various nanocomposites [125]

System Type	Hydrostatic Compression		Hydrostatic Tension	
	$K(\text{GPa})$	% Gain/loss	$K(\text{GPa})$	% Gain/loss
$C_{60}$ - PE	3.529	17.39	3.478	22.29
$C_{180}$ - PE	3.454	14.90	3.272	15.04

It is evident from Table 3 that elastic properties of nanocomposites are improved appreciably with the infusion of bucky-balls in PE matrix, and they are also significantly affected by the size of reinforcing bucky-balls.

## 2.4 Finite Element Modeling

As a very general and powerful numerical analysis tool, finite element method was used to predict mechanical properties of composite materials started in early 1970s [128-129]. Since then, various finite element models have been developed to characterize all kinds of composite materials [e.g. 130-136]. In 1991, Sumio Iijima, a Japanese scientist, discovered carbon nanotubes (CNTs) which possess exceptionally high stiffness and strength, as well as superior electrical and thermal properties [137-139]. Soon after that CNTs were used as reinforcement in developing nanocomposite materials. In the past decade or so, there have been explosively experimental work [e.g. 7, 8, 140-155] and analytical work [e.g. 156-169], as well as finite element modeling work [e.g. 170-198] on developing, analyzing and characterizing CNT reinforced nanocomposites and other nanocomposites. In the following, three finite element modeling approaches will be discussed. They are multiscale representative volume element (RVE) modeling, unit cell modeling, and object-oriented modeling.

### 2.4.1 Multiscale RVE modeling

Liu and Chen [180] extended the RVE concept used by Hyer [199] and Nemat-Nasser and Hori [200] for conventional fiber-reinforced composites at the microscale to nanoscale, and evaluated the effective mechanical properties of CNT-based composites by using a three-dimensional

nanoscale RVE based on elasticity theory and solved by the finite element method. An RVE is composed of a single (or multiple) nanofiller(s) with surrounding matrix material, plus proper boundary conditions to account for the effects of the surrounding materials. It is used as a building block to assemble the composite. Zhang et al. [201] linked continuum analysis with atomistic simulation by incorporating interatomic potential and atomic structures of CNTs directly into the constitutive law. Shi et al. [185] presented a hybrid atomistic/continuum mechanics method to study the deformation and fracture behavior of CNTs embedded in composites. The method is based on a representative unit cell divided into three distinct regions analyzed using an atomistic potential, a continuum method based on the Cuchy–Born rule and a micromechanics method, respectively. Li and Chou [180] proposed a multi-scale modeling approach to study the compressive behavior of CNT/polymer composites. They modeled the nanotube at the atomistic scale and analyzed the matrix deformation using the continuum finite element method. The van der Waals interactions between carbon atoms and the finite element nodes of the matrix were simulated using truss rods.

The multiscale RVE integrates nanomechanics and continuum mechanics, thus bridging the length scales from the nano- through the mesoscale. The procedure of multiscale RVE modeling is exhibited by the work of Tserpes et al. [172] in the following. Tserpes et al. proposed a multiscale RVE to investigate the tensile behavior of CNT/polymer composites. The RVE is a rectangular solid whose entire volume is taken up by the matrix, and the nanotube is modeled as a three-dimensional (3D) elastic beam. The 3D solid elements and beam elements are used to model the matrix and nanotube, respectively. The RVE is synthesized in two steps. First, the behavior of the isolated nanotube is simulated using the progressive fracture model [202]. The concept of the model is based on the assumption that carbon nanotubes, when loaded, behave like space-frame structures. The bonds between carbon atoms are considered as load-carrying members while carbon atoms as joints of the members. The non-linear behavior of the C-C bonds is modeled by the modified Morse interatomic potential [203], and the nanotube structure is modeled by finite element method. Second, the nanotube is inserted into the matrix to form the RVE. The matrix is modeled by solid elements, and the nanotube is represented by 3D elastic beam elements created by binding the nodes of the matrix. The synthesis of the RVE is shown in Fig. 9.

#### ***2.4.2 Unit cell modeling***

The conventional unit cell concept is the same as the RVE [132, 204]. Here we define a unit cell as a special RVE that it has a relatively big size (usually in micrometers) and contains a significant number of fillers (usually in tens to hundreds or more). Such defined unit cell is still the building block of the composite, but as it gets more complicated, analytical models are difficult to establish or too complicated to solve, and numerical modeling and simulation become a necessity.

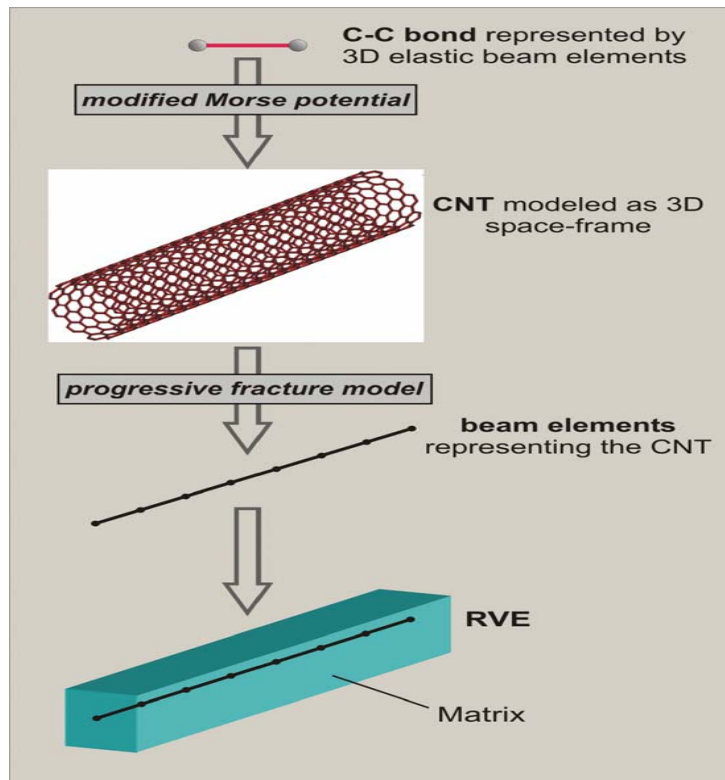


Figure 9. Synthesis of the RVE [172].

The most common method used to characterize the mechanical properties of nanocomposites with unit cell is the finite element method. Hbaieb et al. [177] examined the Young's modulus of nanoclay/polymer nanocomposites with both 2D and 3D unit cells using the finite element method. Four unit cells were created. They are, respectively, 2D and 3D aligned and randomly oriented nanoclay particles models, as shown in Fig. 10. Two kinds of boundary conditions are considered. They are periodic boundary conditions and symmetrical boundary conditions. For the 2D models (both aligned and random cases) the periodic boundary conditions are:

$$u(\text{RE})=u(\text{LE})+\delta_1$$

$$v(\text{RE})=v(\text{LE})$$

$$u(\text{TE})=u(\text{BE})$$

$$v(\text{TE})=v(\text{BE})+\delta_2$$

where RE, LE, TE, BE and  $\delta_1$  and  $\delta_2$  are the right, left, top, bottom edges and the axial and transverse displacements, respectively. The symmetrical boundary conditions for the 2D models are:

$$u(\text{LE})=0$$

$$v(\text{BE})=0$$

$$u(\text{RE})=\delta$$

where  $\delta$  is the given normal displacement in the x direction. In addition, all edges are free of shear traction and the top edge is free of normal traction as well.

For the 3D models (both aligned and random cases) only symmetrical boundary conditions are applied, and they are given as:

$$\begin{aligned} u(\text{LF}) &= 0 \\ v(\text{BF}) &= 0 \\ w(\text{BKF}) &= 0 \\ u(\text{RF}) &= \delta \end{aligned}$$

where LF, BF, BKF and RF stand for left face, bottom face, back face and right face. All other faces are free of any displacement or traction constraints. The numerical results indicated that 2D models do not predict the elastic modulus of clay/polymer nanocomposites accurately. The Mori-Tanaka model [89] gives reasonably accurate predictions of the stiffness of the nanocomposites whose volume fraction is less than 5% for aligned particles but underestimates the stiffness at higher volume fractions. For randomly oriented particles the W-P model [94] overestimates the stiffness of the nanocomposites.

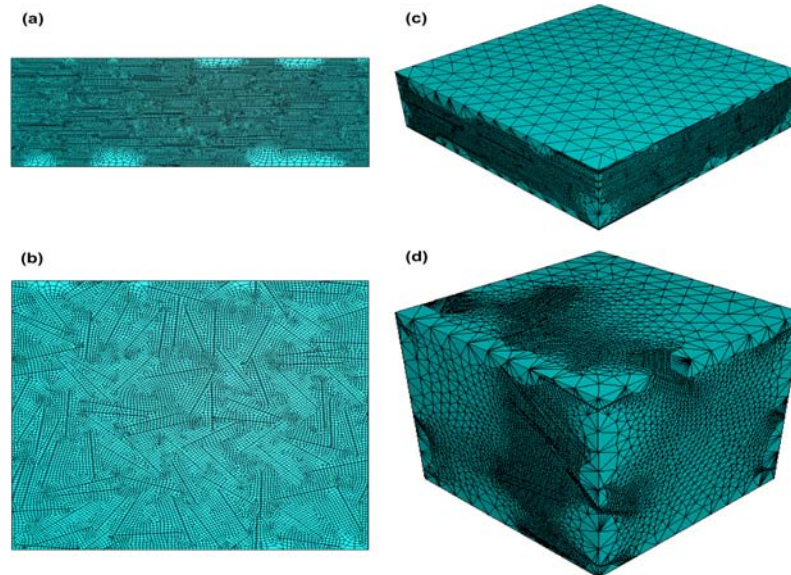


Figure 10. Mesh details of the model for (a) 2D aligned particle distribution, (b) 2D randomly oriented-particle distribution, (c) 3D aligned particle distribution, and (d) 3D randomly oriented-particle distribution. Particle volume fraction is 5%, the particle aspect ratio is 50,  $E_p/E_m=100$ ,  $\nu_m=0.35$ ,  $\nu_p=0.2$ . Subscripts p and m represent particle and matrix, respectively [177].

Recently, Lee et al. [170] used a 3D unit cell model to analyze the deformation behavior of randomly distributed  $\text{Al}_{18}\text{B}_4\text{O}_{33}$  whisker-reinforced  $\text{AS}_{52}$  magnesium alloy matrix composite. The  $\text{Al}_{18}\text{B}_4\text{O}_{33}$  whiskers are  $10 - 30 \mu\text{m}$  long and  $0.5 - 1.0 \mu\text{m}$  in diameter. The dimensions of

the unit cell are  $10 \times 20 \times 20 \mu\text{m}^3$  which contains (fully or partially) 260 whiskers. The volume fraction of the whiskers is 15%. Fig. 11 shows a typical unit cell (with the meshes of the whiskers) and an optical micrograph of the composite. For the Young's modulus and overall elastic-plastic response of the composite, the finite element modeling results are in excellent agreement with the experimental results.

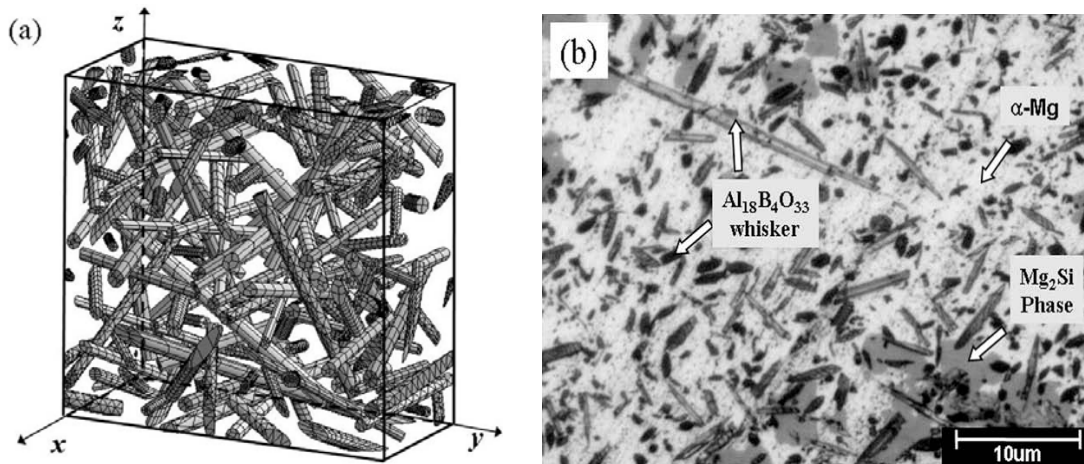


Figure 11. (a) 3D random whisker-reinforced composite model, and (b) an optical micrograph of squeeze-infiltrated  $\text{Al}_{18}\text{B}_4\text{O}_{33}/\text{Mg}$  random whisker composite [170].

### 2.4.3 Object-oriented modeling

In both multiscale RVE modeling and unit cell modeling, two basic assumptions are made. First, nanofillers can be idealized to simple geometries such as spheres, ellipsoids, cylinders, or cubes. And second, nanocomposites can be reproduced by assembling a large number of such RVEs (or unit cells). This can be a serious limitation when dealing with complex and highly heterogeneous nanocomposites. For example, for highly variable and irregular angular structure of fillers, using approximation of simple geometrical particles could not capture the complex morphology, size, and spatial distribution of the reinforcement. Therefore, the object-oriented modeling which is able to capture the actual microstructure morphology of the nanocomposites becomes necessary in order to accurately predict the overall properties.

The object-oriented modeling is a relatively new approach. It incorporates the microstructure images such as scanning electron microscopy (SEM) micrographs into finite element grids. Thus the mesh reproduces exactly the original microstructure, namely the inclusions size, morphology, spatial distribution, and the respective volume fraction of the different constituents. A object-oriented finite element code, OOF [205, 206], developed by National Institute of Standards and Technology (NIST), has been extensively used in analyzing fracture mechanisms and material properties of heterogeneous materials [207-216] and mechanical properties of nanocomposites

[8, 178, 179, 217]. In the following, a 2D object-oriented finite element modeling will be discussed, followed by a 3D modeling.

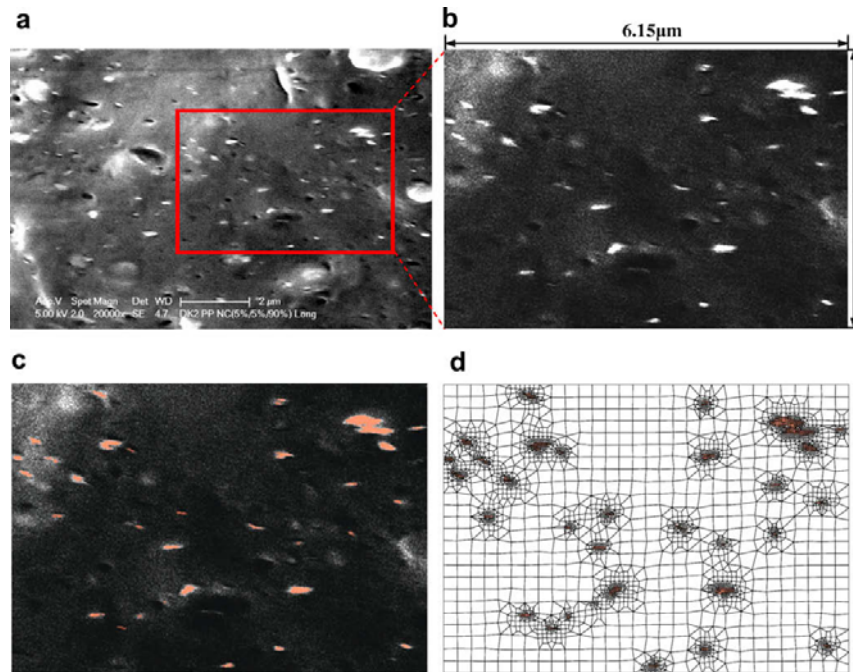


Figure 12. Typical example of creating OOF model of PP/organoclay nanocomposites (5 wt% in clay content): (a) original SEM image, (b) captured SEM image portion, (c) image segmentation using pixel selection, and (d) finite element mesh (highlighted regions contain organoclay particles and the rest are PP matrices) [8].

Dong et al. [8] studied the mechanical properties of polypropylene (PP)/organoclay nanocomposites with different clay contents ranging from 1 to 10 wt%. Their work started with the specimen fabrication through experimental characterization to theoretical predictions and numerical modeling using OOF. SEM micrographs from longitudinal loading direction of the specimen were captured and mapped onto the finite element model, as shown in Fig. 12. The actual nano/microstructures (their size, shape, and distribution etc.) of the PP and the organoclay were used in the computational model, and each phase was attributed the corresponding material properties. The OOF modeling results for the tensile modulus show a good agreement with the experimental data and theoretical predictions.

Chawala et al. [178] used 3D object-oriented finite element modeling to evaluate the mechanical behavior of SiC particle-reinforced Al composites. For a volume of  $100 \times 100 \times 20 \mu\text{m}^3$  cell, there are about 100 SiC particles which produce 20% volume fraction. They compared the

results of the Young's modulus and the stress-strain relations from the object-oriented (microstructure-based) model with the results of the experiment and the numerical results from simplified models (which include rectangular prism, multiparticle-ellipsoids, and multiparticle-spheres, etc.). Some of the results were shown in Fig. 13. Their results indicate that 3D microstructure-based model can accurately predict the properties of particle-reinforced composites, while the simple analytical models can not as they do not account for the microstructural factors that influence the mechanical behavior of the material.

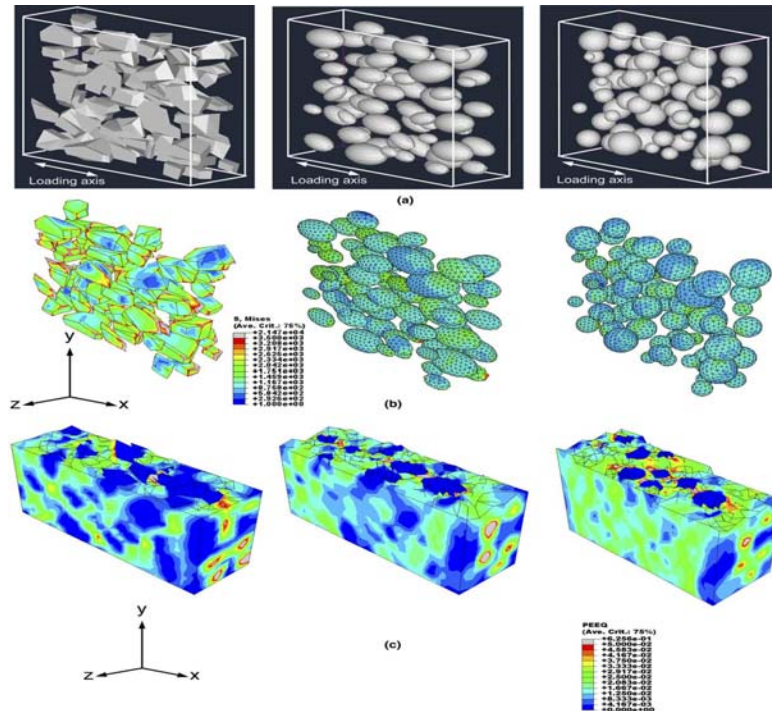


Figure 13. Comparison between 3D finite element models incorporating actual microstructure and approximation to spherical particles: (a) FEM models, (b) von Mises stress distribution in particles, and (c) plastic strain in matrix [178].

### 3. MECHANICAL PROPERTY ENHANCEMENT

Fillers added to matrix can change the mechanical properties of the matrix material. Comparing to traditional composite materials, nanocomposites have the following characterizations:

1. Nanoparticles can substantially improve the mechanical properties of the host matrix materials [140,142,218-220]. Even at very low filler volume content such as 1-5%, a considerable improvement of the mechanical properties can be achieved [143, 221-223].
2. It is observed that for some nanocomposites, with the same filler volume fraction, the stiffness and strength increases as the particle size decreases [125,182, 224-227].

3. In general, the stiffness of nanocomposites tends to increase as the filler volume fraction increases. This function may be nonlinear. There may exist a critical volume fraction beyond which the stiffness starts decrease [228].

For conventional composite materials, micromechanics theories consider that the overall mechanical properties of composites are functions of constituent properties, constituent volume fraction, inclusion shapes and orientations, and state of dispersion. It does not consider the interactions between filler and matrix at their interface. For nanocomposites, the mechanical property enhancement not only depends on the above factors, but also depends on the interaction between the filler and the matrix.

### 3.1 Mechanisms of stiffness and strength enhancement

It is widely accepted that there is an interphase exist between the nanofillers and the matrix material in nanocomposites. This interphase is a transition region, which extends nanometers to micrometers over which the mechanical and physical properties change from the properties of filler to the properties of the matrix. Among many researchers who studied the nanocomposites interphase behavior, Boutaleb et al. [156] investigated the influence of interphase on the overall behavior of silica spherical nanoparticle/polymer composites by means of analytical and finite element methods. Fig. 14 shows a schematic of a composite material containing randomly located spherical nanoparticles (left) and a spherical nanoparticle coated with a graded interphase (right). The interphase is represented as a third phase around the nanoparticles. A model of axisymmetric RVE with periodical boundary conditions was examined. The analysis results show that the interphase is a dominant parameter controlling the overall nanocomposite behavior.

To estimate the elastic modulus of the interphase in polymer nanocomposites, Saber-Samandari and Khatibi [229] developed a 3D unit cell model to represent the three constituent phases including particle, interphase and matrix. The elastic modulus of the interphase at any point,  $r$ , is described by a power law as:

$$E_i(r) = E_m r_i / r + (E_f - E_m r_i / r_f) \left( \frac{r_i - r}{r_i - r_f} \right)^{n/2} \quad (3.1)$$

where  $E_m$  and  $E_f$  are matrix and nanoparticle elastic moduli, respectively,  $r_f$  and  $r_i$  are the filler and interphase radii, and  $n$  is the intragallery enhancement factor which depends on the chemistry and surface treatment of the particles considered.

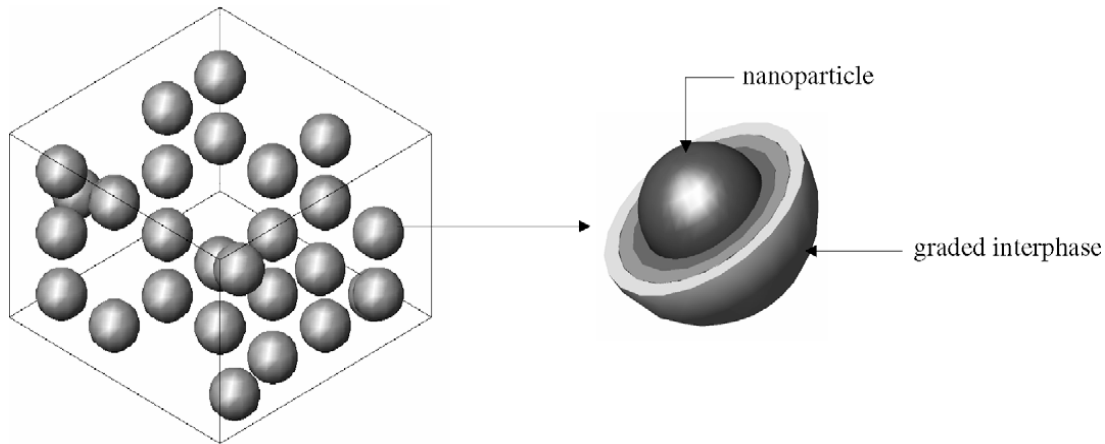


Figure 14. Schematic of a composite material containing randomly located spherical nanoparticles (left) and a spherical nanoparticle coated with an interphase (right) [156].

How exactly the interphase affects the nanocomposites properties is still a research topic. Some intend to think the interphase refined the grain size of matrix leads to smaller critical flaw size and higher strength. Some researchers believe that nanoparticles yield dislocations around them, and these dislocations release residual stresses in the matrix. Thus the defect size along the grain boundaries is reduced. There are also some researchers who think nanofillers impart additional strength of their own to the matrix through the interphase. Nevertheless to say, the strengthening mechanism of nanocomposites is not fully understood. Several mechanical properties of nanocomposites are also improved for the same reason, such as hardness, wear resistance, and thermal shock resistance.

The interaction between nanofillers and matrix is the key to the nanocomposites properties enhancement. There are many factors affecting that interaction, such as the filler volume (weight) fraction, degree of dispersion, the filler geometry and orientation, etc. We assume the same volume fraction and identical degree of dispersion, only the filler geometry (aspect ratio) and orientation will be considered. We define a reactive surface area per unit volume of filler,  $\gamma$ , as

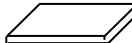
$$\gamma = \frac{A}{V} \quad (3.2)$$

where  $A$  and  $V$  are surface area and volume of the filler, respectively. Table 4 shows the major axis and the  $\gamma$  value for some typical geometry of the nanofillers.

Consider three most common geometries, i.e., sphere (nanoparticles), disk (nanoplatelets, nanolayers), and cylinder (nanotubes, nanofibers). For the cuboid, if  $a=b=c$ , it becomes a cube, close to sphere; if  $a=b \gg c$ , it becomes a platelet; if  $a \gg b \approx c$ , it becomes a rod, close to cylinder. Assume that the diameter of the sphere, the diameter of the cylinder cross-section, and the

thickness of the disk are the same. According to the values in Table 4, the reinforcement efficiency of the three geometries in the major axis direction, from good to poor, is sphere-cylinder-disk. But nanoplatelets are thought to possess better reinforcement effects than those of spherical and fiber-like particles [230].

Table 4.  $\gamma$  value and the major axis for typical filler geometries

Name	Shape	$\gamma$	Parameters
Cylinder		$2\left(\frac{2}{t} + \frac{1}{a}\right) \approx \frac{4}{t}$ as $t \ll a$	t-diameter of cross section area, a-length
Disk-like platelet		$2\left(\frac{1}{t} + \frac{1}{a}\right) \approx \frac{2}{t}$ as $t \ll a$	t-thickness, a-radius
Rectangular platelet		$2\left(\frac{1}{t} + \frac{1}{a} + \frac{1}{b}\right) \approx \frac{2}{t}$ as $t \ll a, b$	t-thickness, a and b-length and width
Sphere		$\frac{6}{t}$	t-diameter
Cuboid		$2\left(\frac{1}{a} + \frac{1}{b} + \frac{1}{c}\right)$	a, b and c-lengths of the three sides
Cone		$3\left(\frac{1}{h} + \sqrt{\frac{1}{h^2} + \frac{4}{t^2}}\right)$	t-base diameter h-height

As the filler orientation is very important in reinforcement, equation (3.2) has to be modified to account for the effect of orientation of the filler surfaces. Now we define an effective surface area per unit volume of filler,  $\bar{\gamma}$ , as

$$\bar{\gamma} = \frac{\bar{A}}{V} \quad (3.3)$$

where  $\bar{A}$  is the effective filler surface area, and it represents the portion of surfaces which is normal to the direction of major axis (see Table 4). The value of  $\bar{\gamma}$  for sphere, disk, and cylinder in the major axis is  $3/2t$ ,  $2/t$ , and  $4/t$ , respectively. Therefore, in the major direction shown, the order of reinforcement efficiency, from good to poor, is cylinder-disk-sphere.

If the nanofillers are randomly oriented, the reinforcement efficiency of nanospheres is probably better than that of nanolayers, and the reinforcement efficiency of nanolayers is probably better

than that of nanocylinders. This is because sphere is isotropic, and disk is transversely isotropic, and cylinder is anisotropic.

For all the geometries of the filler, as the characteristic dimension (the smallest dimension) decreases, the value of  $\gamma$  will increase. That is, the smaller the filler, the better enhancement it will provide. This is similar to the Hall-Petch effect on the strength of metals. Hall-Petch relates the yield stress of a metal to its average grain diameter  $d$  as

$$\sigma_y = \sigma_0 + kd^{-1/2} \quad (3.4)$$

where  $\sigma_0$  and  $k$  are the constants related to the material of interest. The yield stress increases as the grain size decreases. It is also interesting to note that just as Hall-Petch equation does not apply to extremely fine grain sizes, fine size filler enhancement on nanocomposites may also have a limit. Schiotz and Jacobsen [231] investigated nanocrystalline copper, and pointed out that there may be a maximum in the strengthening that can be obtained by decreasing the grain size, so that below a certain critical grain size the strength begins to decrease again as the grain size decreases.

### 3.2 Fracture Toughness

Nanocomposites can not only improve stiffness and strength, but also fracture toughness [232-242]. In general, the fracture toughness of nanocomposites increases as the volume fraction increases, and increases as the nanofiller size decreases. For silica/epoxy nanocomposites, Ragosta et al. [235] found the fracture toughness improved as the volume fraction of 15-nm silica particles increases. Similar results were obtained by Zhang et al. [234] with 25-nm silica particles, and by Chen et al. [232] with 12-nm silica particles. Through experiments and an analytical model, Adachi et al. [233] studied the mode I fracture toughness of silica/epoxy nanocomposites, and found that the toughness increased drastically as the silica volume fraction increased and the particle diameters decreased. In nanocomposites with a low volume fraction of particles, the volume fraction affected the fracture toughness more; and with high volume fractions, the particle size affected the fracture toughness more.

Just as for stiffness and strength, the toughening mechanism of nanocomposites is also mainly from the interaction between the fillers and the matrix. Awaji et al. [243] observed silicon carbide/alumina nanocomposites by transmission electron microscopy (TEM), and found that silicon carbide nanoparticles were dispersed both inside the alumina grains and on the grain boundaries. The fracture toughness is improved by the change of fracture mode from intergranular fracture of monolithic alumina to transgranular fracture of nanocomposites. Fig. 15 shows a schematic illustration of the toughening mechanism [244]. Nanoparticles are dispersed within the matrix grains. Then sub-grain boundaries or dislocation networks are generated around the nanoparticles (Fig. 15A). When the tip of a propagating large crack reaches this area, these dislocations in the matrix will operate as nano-crack nuclei in the vicinity of the

propagating crack tip (Fig. 15B). The highly stressed frontal process zone (FPZ) ahead of the crack tip is then released by nano-crack nucleation, and the nano-cracks expand the FPZ size, enhancing the fracture toughness of the materials [236].

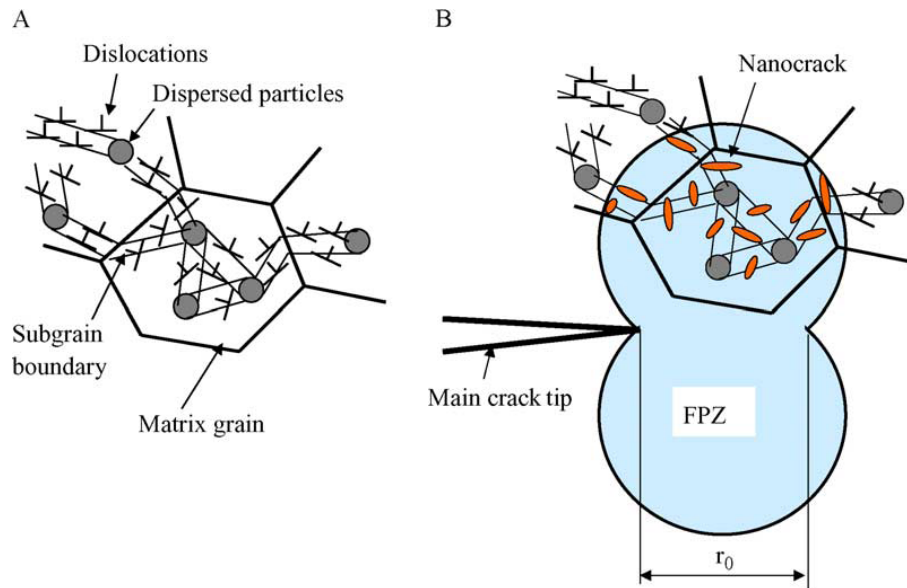


Figure 15. Schematic description of the toughening mechanism in nanocomposites.

(A) Intra-type nano-structure, (B) FPZ creation [244].

#### 4. CONCLUDING REMARKS

Characterizing and modeling mechanical properties of nanocomposites is reviewed and evaluated. Nanocomposites are made by dispersing nanofillers (e.g., silicate and ceramic nanoparticles, CNTs, etc.) into matrix (e.g., some polymers, ceramics, metals, etc.). Comparing with conventional composite materials, nanocomposites have numerous advantages such as high mechanical and physical properties, and high reinforcement efficiency. The high enhancement of mechanical properties of nanocomposites is mainly attributed to the interaction between the nanofillers and the matrix material through the interphase which is a transition region from the nanofillers to the matrix, and the high value of the reactive surface area per unit volume of nanofillers.

Comprehensive understand of the mechanisms of mechanical property enhancement is crucial in order to achieve the longstanding goal of predicting nanoparticles–nanocomposites–property relationships in material design and optimization. Experimental characterizing and nanomechanics-based computer modeling and simulation of mechanical properties of nanocomposites are the two wings in understanding the mechanisms. Many traditional simulation techniques have been employed, and some novel simulation techniques have been

developed to study nanocomposites. These techniques represent approaches at various time and length scales from molecular scale to microscale, and then to macroscale, and have shown success to various degrees in addressing many aspects of nanocomposites. The simulation techniques developed thus far have different strengths and weaknesses, depending on the need of research. Despite substantial progress made in the past decade, there are a number of challenges in computer modeling and simulation. New concepts, theories and computational tools should be developed. In general, there are two fronts that should be pointed out. First, there is a need to develop new and improved simulation techniques at individual time and length scales. Secondly, it is important to integrate the developed methods at wider range of time and length scales, spanning from quantum domain to molecular domain, to mesoscopic domain, and finally to macroscopic domain, to form a useful tool for exploring the structural and mechanical properties, as well as optimizing design of nanocomposites [100]. Specific challenges and the solution strategies are discussed in the following:

1. In either developing new or characterizing the current exist nanocomposites, a comprehensive approach should be adopted that integrates the experimental techniques with nanomechanics-based analytical explorations and computer modeling and simulation.
2. New computational tools are specially needed in the area of multiscale RVE modeling. The multiscale RVE modeling is in nature a “local-global” approach. In order to catch the local nano/micro characteristics, quantum mechanics or molecular dynamics needs to be explored. But the prediction of global macro-mechanical properties requires the continuum mechanics-based finite element method. How to transit from local to global becomes a research issue. Ogata et al. [198] proposed a way of combing quantum mechanics, molecular dynamics, and finite elements. In regions where the atoms obey the laws of continuum mechanics, the finite element method is used. However, in critical areas such as the extremity of a fracture, molecular dynamics and even quantum mechanics are required to obtain a more detailed study of the fracture process. The transition from the global to local levels involves a change of scale. Xiao and Belytschko [245] proposed a way of improving the numerical compatibility between regions modeled by molecular dynamics and those modeled using the finite element method. The suggested method is introducing a broad transition region by superposing the finite element mesh of the continuum region on the atomistic structure of the molecular dynamics region. Clearly, there is still a lot of work needs to be done in connecting the local parameters to the global parameters.
3. In object-oriented finite element modeling, 2D modeling has been extensively used in nanocomposites [e.g. 8, 179, 217], and there are also some works on 3D modeling [e.g. 178]. There are still issues to be resolved in 3D modeling, especially advanced object-oriented 3D finite element codes.

## ACKNOWLEDGEMENTS

This work was supported by the funding from the Air Force Office of Scientific Research and the Department of Defense Research & Engineering Office with grant number FA9550-08-1-0230. The first two authors would also like to acknowledge the significant interaction and support from Drs. Jennifer Stewart-Wright and Evelyn Maria Thompson from Tennessee State University.

## APPENDIX

### Formulas Related to the Overall Moduli:

$$\alpha = \frac{1}{3}T_{ijj} = \frac{F_1}{F_2}$$

$$\beta = \frac{1}{5}(T_{ijj} - \frac{1}{3}T_{ijj}) = \frac{1}{5}\left(\frac{2}{F_3} + \frac{2}{F_4} + \frac{F_5 - F_1}{F_2}\right)$$

$$\varphi = \frac{1}{3F_2}(2F_6A_1 + 6F_6B_1 + F_7A_2 + 3F_7B_2)$$

$$\psi = \frac{1}{5F_2}(F_8A_1 + F_9A_2 + 2F_6B_1 + F_7B_2) + \frac{2}{5}\left(\frac{A_3}{F_4} + \frac{A_4}{F_3}\right) - \frac{\varphi}{5}$$

where

$$F_1 = 1 + \frac{1}{3}\left[\frac{1}{2}(1-R)(3f + 9\theta - 4) + 2R(1-\theta)\right]A_1 + \frac{1}{3}\left[(1-R)(2 + 3f) + R(2-\theta)\right]A_2 + \frac{1}{3}(3-4R)(3\theta-2)(B_1 - B_2)$$

$$F_2 = 1 + \frac{1}{2}(1-R)(f + 3\theta)A_1 + [(1-R)(1+f) + R(1-\theta)]A_2 + (3-4R)[\theta B_1 + (1-\theta)B_2] + \frac{1}{2}(3-4R)[f + \theta - R(f - \theta + 2\theta^2)](A_1A_2 + A_1B_2 + 2B_1A_2)$$

$$F_3 = 1 + [1 - (f + \frac{3}{2}\theta) + R(f + \theta)]A_4$$

$$F_4 = 1 + 0.25[f + 3\theta + R(\theta - f)]A_3$$

$$F_5 = 2 + \frac{1}{2}(1-R)(f + 3\theta)A_1 + [(1-R)(1+f) + R(1-\theta)]A_2 + (3-4R)[\theta B_1 + (1-\theta)B_2]$$

$$F_6 = 1 + \frac{1}{2}[(1-R)(2 + 3f) + R(2-\theta)]A_2 + \frac{1}{2}(3-4R)(2-3\theta)B_2$$

$$F_7 = 1 + \frac{1}{2}[(1-R)(3f + 9\theta - 4) + 4R(1-\theta)]A_1 + (3-4R)(3\theta-2)B_1$$

$$F_8 = 1 + [(1-R)(1+f) + R(1-\theta)]A_2 + (3-4R)(1-\theta)B_2$$

$$F_9 = 1 + \frac{1}{2}(1-R)(f+3\theta)A_1 + \theta(3-4R)B_1$$

The constants  $R$ ,  $A_i$  ( $i=1, 2, 3, 4$ ) and  $B_i$  ( $i=1, 2$ ) are non-dimensional ones related to the elastic constants of the isotropic matrix and the transversely isotropic inhomogeneity.

$$R = \frac{3\mu_m}{3K_m + 4\mu_m}$$

$$A_1 = \frac{k_f - l_f}{\mu_m} - 1, \quad A_2 = \frac{n_f - l_f}{2\mu_m}, \quad A_3 = \frac{m_f}{\mu_m} - 1, \quad A_4 = \frac{p_f}{\mu_m} - 1$$

$$B_1 = \frac{2k_f + l_f}{9K_m} - \frac{2k_f - 2l_f}{6\mu_m}, \quad B_2 = \frac{n_f + 2l_f}{9K_m} - \frac{n_f - l_f}{6\mu_m}$$

where  $k$ ,  $n$ ,  $m$ ,  $p$ , and  $l$  are the notations adopted by Hill. They can be expressed in general by stiffness tensor components as

$$k = \frac{1}{2}(C_{2222} + C_{2233}), \quad n = C_{1111}, \quad m = \frac{1}{2}(C_{2222} - C_{2233}), \quad p = C_{1212}, \quad l = C_{1122}$$

For an isotropic material, the above constants degenerate into

$$k = K + \frac{1}{3}\mu, \quad n = K + \frac{4}{3}\mu, \quad m = p = \mu, \quad l = K - \frac{2}{3}\mu$$

$f$  and  $\theta$  are related to the geometry of the spheroidal inhomogeneity, which are

$$f = \begin{cases} \frac{\chi^2}{1-\chi^2}(3\theta-2), & \chi = c/a < 1 \text{ for oblate spheroid, } a_2 = a_3 = a > a_1 = c \\ \frac{\chi^2}{\chi^2-1}(2-3\theta), & \chi = c/a > 1 \text{ for prolate spheroid, } a_1 = a < a_2 = a_3 = c \end{cases}$$

$$\theta = \begin{cases} \frac{\chi}{(1-\chi^2)^{3/2}} \{\cos^{-1} \chi - \chi(1-\chi^2)^{1/2}\} & \text{for oblate spheroid} \\ \frac{\chi}{(\chi^2-1)^{3/2}} \{\chi(\chi^2-1)^{1/2} - \cosh^{-1} \chi\} & \text{for prolate spheroid} \end{cases}$$

## REFERENCES

- [1] Braun T, Schubert A, Zsindely S. Nanoscience and nanotechnology on the balance. *Scientometrics* 1997;38:321–325.
- [2] Alexandre M, Dubois P. Polymer-layered silicate nanocomposites: preparation, properties and uses of a new class of materials. *Mater Sci Eng* 2000;28:1–63.
- [3] Herron N, Thorn DL. Nanoparticles: uses and relationships to molecular clusters. *Adv Mater* 1998;10:1173–84.

- [4] Kumar AP, Depan D, Tomer NS, Singh RP. Nanoscale particles for polymer degradation and stabilization-Trends and future perspectives. *Progress in Polymer Science*, 2009; 34: 479-515.
- [5] Vaia RA, Wagner HD. Framework for nanocomposites. *Mater Today* 2004;7:32-7.
- [6] Liu H, Brinson LC. Reinforcing efficiency of nanoparticles: A simple comparison for polymer nanocomposites. *Compos Sci Technol* 2008; 68: 1502-1512.
- [7] Thilly L, Petegem SV, Renault PO, Lecouturier F, Vidal V, Schmitt B, Swygenhoven V. A new criterion for elastio-plastic transition in nanomaterials: Application to size and composite effects on Cu-Nb nanocomposite wires. *Acta Materialia* 2009; 57: 3157-3169.
- [8] Dong Y, Bhattacharyya D, Hunter, PJ. Experiental Characterisation and object-oriented finite element modeling of polypropylene/organoclay nanocomposites. *Comp Sci Technol* 2008; 68: 2864-2875.
- [9] Chen Q, Chasiotis I, Chen C, Roy A. Nanoscale and effective mechanical behavior and fracture of silica nanocomposites. *Comp Sci Technol*. 2008; 68: 3137-3144.
- [10] Chen WH, Cheng HC, Hsu YC, Uang RH, Hsu JS. Mechanical material characterization of Co nanowires and their nanocomposite. *Comp Sci Technol* 2008; 68: 3388-3395.
- [11] Song SY, Youn JR. Modelling of effective elastic properties of polymer based carbon nanotube composites. *Polymer* 2006; 47, 1741-1748.
- [12] Schuster, BE, Wei Q, Ervin MH, Hruszkewycz SO, Miller MK, Hufnagel TC, Ramesh KT. Bulk and microscale compressive properties of a pd-based metallic glass. *Scripta Materialia* 2007; 57 (6), 517-520.
- [13] Zhang H, Schuster BE, Wei Q, Ramesh KT. The design of accurate micro-compression experiments. *Scripta Materialia* 2006, 54(2), 181-186.
- [14] Chang NK, Lin YS, Chen CY, Chang SH. Size effect of indenter on determining modulus of nanowires using nanoindentation technique. *Thin Solid Films* 2009; 517: 3695-3697.
- [15] Poon B, Rittel D, Ravichandran D. An analysis of nanoindentation in linearly elastic solids. *Int. J. Solids Struct*. 2008; 45: 6018-6033.
- [16] Han CF, Lin JF. Modeling to evaluate the contact areas of hard materials during the nano-indentation tests. *Sensors Actuators A* 2008; 147(1): 229-241.
- [17] Ling Z, Hou J. A nanoindentation analysis of the effects of microstructures on elastic properties of Al<sub>2</sub>O<sub>3</sub>/SiC composites. *Comp. Sci. Technol*. 2007; 67: 3121-3129.
- [18] Lee SH, Wang S, Pharr GM, Xu H. Evaluation of interphase properties in a cellulose fiber-reinforced polypropylene composite by nanoindentation and finite element analysis. *Composites: Part A* 2007; 38: 1517-1524.
- [19] Qi HJ, Teo KBK, Lau KKS, Boyce MC, Milne WI, Robertson J, Gleason KK. Determination of mechanical properties of carbon nanotubes and vertically aligned carbon nanotube forests using nanoindentation. *J. Mech. Phy. Solids*. 2003; 51: 2213-2237.
- [20] Li X, Bhushan B. A review of nanoindentation continuous stiffness measurement technique and its applications. *Mater Charact*. 2002; 48:11-36.

- [21] Gao SL, Mader E. Characterisation of interphase nanoscale property variations in glass fiber reinforced polypropylene and epoxy resin composites. *Composites: Part A* 2002; 33:559–576.
- [22] Hodzic A, Stachurskia ZH, Kim JK. Nano-indentation of polymer–glass interfaces part I experimental and mechanical analysis. *Polymer* 2000;41:6895–905.
- [23] Downing TD, Kumar R, Cross WM, Kjerengtroen L, Kellar JJ. Determining the interphase thickness and properties in polymer matrix composites using phase imaging atomic force microscopy and nanoindentation. *J Adhes Sci Technol* 2000;14:1801–12.
- [24] Munz M, Sturm H, Schulz E, Hinrichsen G. The scanning force microscope as a tool for the detection of local mechanical properties within the interphase of fiber reinforced polymers. *Composites: Part A* 1998; 29A:1251–9.
- [25] Oliver WC, Pharr GM. An improved technique for determining hardness and elastic modulus using load and displacement sensing indentation experiments. *J Mater Res* 1992; 7(6):1564–83.
- [26] Fong H, Sarikaya M, White SN, Snead ML. Nanomechanical properties profiles across dentin—enamel junction of human incisor teeth, *Mater. Sci. Eng.* 2000; C7: 119—128.
- [27] Zysset PK, Guo XE, Hoffler CE, Moore KE, Goldstein SA. Elastic modulus and hardness of cortical and trabecular bone lamellae measured by nanoindentation in the human femur, *J. Biomech.* 1999; 32: 1005—1012.
- [28] Habelitz S, Marshall GW, Balooch M, Marshall SJ. Nanoindentation and storage of teeth, *J. Biomech.* 2002; 35: 995—998.
- [29] Cuy JL, Mann AB, Livi KJ, Teaford MF, Weihs TP. Nanoindentation mapping of the mechanical properties of human molar tooth enamel. *Arch. Oral Biol.* 2002; 47: 281—291.
- [30] Marshall GW, Balooch M, Gallagher RR, Gansky SA, Marshall SJ. Mechanical properties of the dentinoenamel junction: AFM studies of nanohardness, elastic modulus, and fracture. *J. Biomedic. Res.* 2001; 54: 87—95.
- [31] Poolthong S, Mori T, Swain MV. Determination of elastic modulus of dentin by small spherical diamond indenters. *J. Dent. Mater.* 2001; 20: 227—236.
- [32] Habelitz S, Marshall SJ, Marshall GW, Balooch M. Mechanical properties of human dental enamel on the nanometer scale. *Arch. Oral Biol.* 2001; 46: 173—183.
- [33] Xu HHK, Smith DT, Jahanmir S, Romberg E, Kelly JR, Thompson VP, Rekow ED. Indentation damage and mechanical properties of human enamel and dentin. *J. Dent. Res.* 1998; 77: 472—480.
- [34] Kinney JH, Balooch M, Marshall SJ, Marshall GW, Wehs TP. Atomic force microscope measurements of the hardness and elasticity of peritubular and intertubular human dentin. *J. Biomech. Eng.* 1996; 118: 133—135.
- [35] Meredith N, Sherriff M, Setchell DJ, Sivanson SAV. Measurements of the microhardness and Young modulus of human enamel and dentin using an indentation technique. *Arch. Oral Biol.* 1996; 41: 539—545.

- [36] Kinney JH, Balooch M, Marshall SJ, Marshall GW, Weihs TP. Hardness and Young's modulus of peritubular and intertubular dentine. *Arch. Oral Biol.* 1996; 41: 9-13.
- [37] van Meerbeek B, Willems G, Celis JP, Roos JR, Braem M, Lambrechts P, Vanherle G. Assessment by nanoindentation of the hardness and elasticity of the resin—dentin bonding area. *J. Dent. Res.* 1993; 72: 1434—1442.
- [38] Toparli M, Koksall NS. Hardness and yield strength of dentin from simulated nano-indentation tests. *Comp Meth Progr Biomed* 2005; 77, 253-257.
- [39] Shin C, Jin HH, Kim MW. Evaluation of the depth-dependent yield strength of a nanoindented ion-irradiated Fe–Cr model alloy by using a finite element modeling. *J. Nucl. Mater.* 2009; 392(3): 476-481.
- [40] Li B, Gu YD, English R, Rothwell G, Ren XJ. Characterisation of nonlinear material parameters of foams based on indentation tests. *Mater. Design* 2009; 30(7): 2708-2714.
- [41] Wang, T.H., Fang, T.H., Lin, Y.C. A numerical study of factors affecting the characterization of nanoindentation on silicon. *Mater. Sci. Eng.* 2006; 447: 244–253.
- [42] Pelletier H, Krier J, Mille P. Characterization of mechanical properties of thin films using nanoindentation test. *Mech. Mater.* 2006; 38: 1182-1198.
- [43] Yu, N., Polycarpou, A.A., Conry, T.F. Tip-radius effect in finite element modeling of sub-50 Nm shallow nanoindentation. *Thin Solid Films* 2004; 450, 295–303.
- [44] Dao M, Chollacoop N, Vliet KJV, Venkatesh TA, Suresh S. Computational modeling of the forward and reverse problems in instrumented sharp indentation. *Acta Mater.* 2001; 49, 3899–3918.
- [45] Zhang W, Subhash G. Finite element analysis of interacting Vickers indentations on brittle materials. *Acta Mater.* 2001; 49 (15): 2961-2974.
- [46] Zhang W, Subhash G. An elastic–plastic-cracking model for finite element analysis of indentation cracking in brittle materials. *Int. J. Solids Struct.* 2001; 38(34/35): 5893-5913.
- [47] Lichinchi, M., Lenardi, C., Haupta, J., Vitalib, R. Simulation of Berkovich nanoindentation experiments on thin films using finite element method. *Thin Solid Films* 1998; 312: 240–248.
- [48] Gan L, Ben-Nissan B. The effects of mechanical properties of thin films on nano-indentation data: Finite element analysis. *Comp. Mater. Sci.* 1997; 8: 273-281.
- [49] Zeng K, Giannakopoulos AE, Rowcliffe DJ. Vickers indentations in glass—II. Comparison of finite element analysis and experiments. *Acta Metallur. Mater.* 1995; 43: 1945-1954.
- [50] Kral ER, Komvopoulos K, Bogy DB. Elastic–plastic finite element analysis of repeated indentation of a half-space by a rigid sphere. *J. Appl. Mech.* 1993; 75: 829–841.
- [51] Wang HF, Yang X, Bangert H, Torzicky P, Wen L. Two-dimensional finite element method simulation of Vickers indentation of hardness measurements on TiN-coated steel. *Thin Solid Films* 1992; 214: 68-73.
- [52] Maritza GJ. Veprek-Heijman, Ratko G. Veprek, Ali S. Argon, David M. Parks and Stan Veprek. Non-linear finite element constitutive modeling of indentation into super- and ultrahard materials: The plastic deformation of the diamond tip and the ratio of hardness to

- tensile yield strength of super- and ultrahard nanocomposites. *Surf. Coat. Technol.* 2009; 203: 3385-3391.
- [53] Jiang W, Batra RC. Identification of elastic constants of FCC metals from 2D load-indentation curves. *Comp. Mater. Sci.* 2009; 45(2): 511-515.
- [54] Harsono E, Swaddiwudhipong S, Liu ZS. Material characterization based on simulated spherical-Berkovich indentation tests. *Scrip. Mater.* 2009; 60(11): 972-975.
- [55] Geng K, Yang F, Grulke EA. Nanoindentation of submicron polymeric coating systems. *Mater. Sci. Eng. A.* 2008; 479(1/2): 157-163.
- [56] Farrissey LM, McHugh PE. Determination of elastic and plastic material properties using indentation: Development of method and application to a thin surface coating. *Mater. Sci. Eng A* 2005; 399: 254-266.
- [57] Zeng K, Soderlund E, Giannakopoulos AE, Rowcliffe DJ. Controlled indentations: a general approach to determine mechanical properties of brittle materials. *Acta Mater.* 1996; 44: 1127-1141.
- [58] Yoshino M, Aoki T, Chandrasekaran N, Shirakashi T, Komanduri R. Finite element simulation of plane strain plastic-elastic indentation on single-crystal silicon. *Int. J. Mech. Sci.* 2001; 43 (2): 313-333.
- [59] Fisher FT, Brinson LC. Nanomechanics of nanoreinforced polymers. In: Rieth M, Schommers W, editors. *Handbook of theoretical and computational nanoscience*. American Scientific Publishers; 2006. 253-360.
- [60] Moniruzzaman M, Winey KI. Polymer nanocomposites containing carbon nanotubes. *Macromolecules* 2006;39(16):5194-5205.
- [61] Thostenson ET, Li CY, Chou TW. Nanocomposites in context. *Compos Sci Technol* 2005;65: 491-516.
- [62] Ajayan PM, Schadler LS, Braun PV. *Nanocomposite science and technology*. Weinheim: WILEY-VCH Verlag GmbH & Co. KGaA; 2003.
- [63] Srivastava D, Wei CY, Cho K. Nanomechanics of carbon nanotubes and composites. *Appl Mech Rev* 2003; 56: 215-30.
- [64] Leamy MJ. Bulk dynamic response modeling of carbon nanotubes using an intrinsic finite element formulation incorporating interatomic potentials. *Int J Solids Struct* 2007; 44: 874-94.
- [65] Odegard GM, Gates TS. Modeling and testing of the viscoelastic properties of a graphite nanoplatelet/epoxy composite. *J Intell Mater Syst Struct* 2006;17: 239-46.
- [66] Sears A, Batra RC. Buckling of multiwalled carbon nanotubes under axial compression. *Phys Rev B* 2006; 73:085410-1-085410-11.
- [67] Arroyo M, Belytschko T. Continuum mechanics modeling and simulation of carbon nanotubes. *Meccanica* 2005;40(4-6):455-69.
- [68] Odegard GM, Clancy TC, Gates TS. Modeling of the mechanical properties of nanoparticle/polymer composites. *Polymer* 2005; 46: 553-62.

- [69] Arroyo M, Belytschko T. Finite element methods for the non-linear mechanics of crystalline sheets and nanotubes. *Int J Numer Methods Eng* 2004;59(3):419–56.
- [70] Zhu LJ, Narh KA. Numerical simulation of the tensile modulus of nanoclay-filled polymer composites. *J Polym Sci* 2004; 42: 2391–406.
- [71] Wu YP, Jia QX, Yu DS, Zhang LQ. Modeling Young's modulus of rubber–clay using composite theories. *Polym Testing* 2004; 23: 903–9.
- [72] Luo J-J, Daniel IM. Characterization and modeling of mechanical behaviour of polymer/clay nanocomposites. *Compos Sci Technol* 2003;63:1607–16.
- [73] Fornes TD, Paul DR. Modeling properties of nylon 6/clay nanocomposites using composite theories. *Polymer* 2003;44:4993–5013.
- [74] Voigt W. Über die beziehung zwischen den beiden elasticitatsconstanten isotroper korper. *Ann Phys* 1889; 38:573–87.
- [75] Reuss A. Berechnung der fliebgrenze von mischkristalen auf grund der plastizitatsbedingung fur einkristalle. *ZAMM* 1929; 9:49–58.
- [76] Hashin Z, Shtrikman, S. A variational approach to the theory of the elastic behavior of multiphase materials. *J Mech Phys Solids* 1963; 11: 127-40.
- [77] Hashin Z, Analysis of composite materials-a survey. *J. Appl. Mech.* 1983; 50: 481-505.
- [78] Halpin JC. Primer on composite materials: analysis. Lancaster: Technomic Publishing Company; 1984.
- [79] Halpin JC, Kardos JL. The Halpin-Tsai equations: a review. *Polym Eng Sci* 1976; 16: 344-52.
- [80] Halpin JC. Stiffness and expansion estimates for oriented short fiber composites. *J Compos Mater* 1969; 3:742-4.
- [81] Halpin JC, Tsai SW. Effect of environmental factors on composite materials; Air Force Technical Report AFML-TR 67-423. Dayton, OH: Wright Aeronautical Laboratories; 1967.
- [82] Hermans JJ. The elastic properties of fiber oriented materials when the fibers are aligned. *Proc Kon Ned Akad v Wetensch B* 1967; 65: 1-9.
- [83] Hill R. Theory of mechanical properties of fibre-strengthened materials: I elastic behaviour. *J Mech Phys Solids* 1964; 12: 199-212.
- [84] Mori T, Tanaka K. Average stress in matrix and average elastic energy of materials with misfitting inclusions. *Acta Metall* 1973; 21:571–4.
- [85] Eshelby JD. The determination of the elastic field of an ellipsoidal inclusion and related problems. *Proc R Soc London A* 1957; 241:376–96.
- [86] Taya M, Mura T. On stiffness and strength of an aligned short-fiber reinforced composite containing fiber-end cracks under uniaxial applied stress. *J Appl Mech* 1981; 48: 361-7.
- [87] Taya M, Chou T-W. On two kinds of ellipsoidal inhomogeneities in an infinite elastic body: an application to a hybrid composite. *Int J Solids Struct* 1981; 17: 553-63.
- [88] Weng GJ. Some elastic properties of reinforced solids, with special reference to isotropic ones containing spherical inclusions. *Int J Engng Sci* 1984; 22 :845-56.

- [89] Tandon GP, Weng GJ. The effect of aspect ratio of inclusions on the elastic properties of unidirectionally aligned composites. *Polym Compos* 1984;5:327–33.
- [90] Hui CY, Shia D. Simple formulae for the effective moduli of unidirectional aligned composites. *Polym Eng Sci* 1998;38:774–82.
- [91] Shia D, Hui CY, Burnside SD, Giannelis EP. An interface model for the prediction of Young's modulus of layered silicate-elastomer nanocomposites. *Polym Compos* 1998;19:608–17.
- [92] Qiu YP, Weng GJ. On the application of Mori-Tanaka's theory involving transversely isotropic spheroidal inclusions. *Int J Eng Sci* 1990; 28: 1121-37.
- [93] Chen T, Dvorak GJ, Benveniste Y. Mori-Tanaka estimate of the overall elastic moduli of certain composite materials. *J Appl Mech* 1992; 59: 539-46.
- [94] Wang J, Pyrz R. Prediction of the overall moduli of layered silicate-reinforced nanocomposites-part I: basic theory and formulas. *Compos Sci Tech* 2004;64:925-934.
- [95] Cox HL. The elasticity and strength of paper and other fibrous materials. *Brit J Appl Phys* 1952; 3: 72-9.
- [96] Tucker III CL, Liang E. Stiffness prediction for unidirectional short-fiber composites: Review and evaluation. *Compos Sci Tech* 1999; 59: 655-671.
- [97] Van Es M, Xiqiao F, Van Turnhout, Van der Giessen E. Comparing polymer-clay nanocomposites with conventional composites using composite modeling. In: Al-Malaika S, Golovoy AW, editors. *Specially polymer additives: principles and applications*. CA Malden, MA: Blackwell Science; 2001. Chapter 21.
- [98] Rapaport DC. *The Art and Science of Molecular Dynamics Simulation*. Cambridge: Cambridge University Press; 2004.
- [99] Frenkel D, Smit B. *Understanding molecular simulation: from algorithms to applications*. 2nd ed. San Diego: Academic Press; 2002.
- [100] Zeng QH, Yu AB, Lu GQ. Multiscale modeling and simulation of polymer nanocomposites. *Prog. Polym. Sci.* 2008; 33: 191–269
- [101] Cornwell CF, Wille LT. Elastic properties of single-walled carbon nanotubes in compression. *Solid State Commun* 1997;101:555–8.
- [102] Zhu R, Pan E, Roy AK. Molecular dynamics study of the stress-strain behavior of carbon-nanotube reinforced Epon 862 composites. *Mater Sci Eng A* 2007; 447: 51-57.
- [103] Mokashi VV, Qian D, Liu YJ. A study on the tensile response and fracture in carbon nanotube-based composites using molecular mechanics. *Compos Sci Technol* 2007;67:530–40.
- [104] Zheng QB, Xue QZ, Yan KO, Hao LZ, Li Q, Gao XL. Investigation of molecular interactions between SWNT and polyethylene/polypropylene/polystyrene/ polyaniline molecules. *J Phys Chem C* 2007;111:4628–35.
- [105] Sun X, Zhao W. Prediction of stiffness and strength of single-walled carbon nanotubes by molecular-mechanics based finite element approach. *Mater Sci Eng* 2005; 390: 366-71.

- [106] Xiao JR, Gama BA, Gillespie Jr JW. An analytical molecular structural mechanics model for the mechanical properties of carbon nanotubes. *Int J Solids Struct* 2005; 42: 3075-92.
- [107] Bao WX, Zhu CC, Cui WZ. Simulation of Young's modulus of single-walled carbon nanotubes by molecular dynamics. *Physica B*. 2004; 352: 156-63.
- [108] Saether E, Frankland SJV, Pipes RB. Transverse mechanical properties of single-walled carbon nanotube crystals. Part I: determination of elastic moduli. *Compos Sci Tech* 2003;63:1543-50.
- [109] Odegard GM, Gates TS, Wise KE, Park C, Siochi EJ. Constitutive modeling of nanotube-reinforced polymer composites. *Compos Sci Tech* 2003; 63: 1671-87.
- [110] Scarpa F, Adhikari S, Phani AS. Effective elastic mechanical properties of single layer grapheme sheets. *Nanotechnology* 2009; 20: 065709.
- [111] Hemmasizadeh A, Mahzoon M, Hadi E, Khandan R. A method for developing the equivalent continuum model of single layer grapheme sheet. *Thin Solid Films* 2008; 516: 7636-40.
- [112] Cho J, Luo JJ, Danial IM. Mechanical characterization of graphite/epoxy nanocomposites by multi-scale analysis. *Compos Sci Tech* 2007; 67: 2399-407.
- [113] Prathab B, Subramanian V, Aminabhavi TM. Molecular dynamics simulations to investigate polymer-polymer and polymer-metal oxide interactions. *Polymer* 2007;48: 409-16.
- [114] Suter JL, Coveney PV, Greenwell HC, Thyveetil MA. Large-scale molecular dynamics study of montmorillonite clay: emergence of undulatory fluctuations and determination of material properties. *J Phys Chem C* 2007;111: 8248-59.
- [115] Ward DK, Curtin WA, Qi Y. Mechanical behavior of aluminum-silicon nanocomposites: A molecular dynamics study. *Acta Materialia* 2006; 54: 4441-51.
- [116] Patel RR, Mohanraj R, Pittman CU. Properties of polystyrene and polymethyl methacrylate copolymers of polyhedral oligomeric silsesquioxanes: a molecular dynamics study. *J Polym Sci Part B: Polym Phys* 2006;44: 234-48.
- [117] Bizet S, Galy J, Gerard JF. Molecular dynamics simulation of organic-inorganic copolymers based on methacryl-POSS and methyl methacrylate. *Polymer* 2006;47:8219-27.
- [118] Minisini B, Tsobnang F. Molecular dynamics study of specific interactions in grafted polypropylene organomodified clay nanocomposite. *Compos Part A: Appl Sci Manuf* 2005;36:539-44.
- [119] Sen TZ, Sharaf MA, Mark JE, Kloczkowski A. Modeling the elastomeric properties of stereoregular polypropylenes in nanocomposites with spherical fillers. *Polymer* 2005;46:7301-8.
- [120] Lau K, Gu C, Hui D. A critical review on nanotube and nanotube/nanoclay related polymer composite materials. *Composites: Part B* 2006; 37: 425-436.
- [121] Smith W, Forester TR. DLPOLY-2.14 manual; 2004. Internet Source: [http://www.cse.clrc.ac.uk/msi/software/DL\\_POLY/MANUALS/USRMAN2.pdf](http://www.cse.clrc.ac.uk/msi/software/DL_POLY/MANUALS/USRMAN2.pdf).

- [122] Smith W, Forester TR. DL\_POLY\_2.0: A general-purpose parallel molecular dynamics simulation package. *J Mol Graph* 1996; 14: 136-41.
- [123] Plimpton SJ. LAMMPS Documentation. Internet Source: <http://www.cs.sandia.gov/~sjplimp/lammps/doc/Manual.html>.
- [124] Ponder JW. TINKER: Software tools for molecular design, Version 3.8. Washington University School of Medicine; 1998.
- [125] Adnan A, Sun CT, Mahfuz H. A molecular dynamics simulation study to investigate the effect of filler size on elastic properties of polymer nanocomposites. *Compos Sci Technol* 2007;67:348–56.
- [126] Mayo SL, Olafson BD, Goddard III WA. DREIDING: A generic force field for molecular simulations. *J Phys Chem* 1990; 94: 8897–909.
- [127] Binder K. Monte carlo and molecular dynamics simulations in polymer science. New York: Oxford University Press; 1995.
- [128] Broutman LJ, Panizza G. Micromechanics studies of rubber-reinforced glassy polymers. *Int J Polymeric Mat* 1971; 1: 95-109.
- [129] Agarwal BD, Broutman LJ. Three-dimensional finite element analysis of spherical particle composites. *Fibre Sci Tech* 1974; 7: 63-77.
- [130] Needleman A. A continuum model for void nucleation by inclusion debonding. *J Appl Mech* 1987; 54: 525-531.
- [131] Christman T, Needleman A, Suresh S. An experimental and numerical study of deformation of metal-ceramic composites. *Acta Metall Mater* 1989; 37: 3029-50.
- [132] Llorca J, Needleman A, Suresh S. An analysis of the effects of matrix void growth on deformation and ductility in metal-ceramic composites. *Acta Metall Mater* 1991; 39: 2317-35.
- [133] Tvergaard V. Analysis of tensile properties for a whisker-reinforced metal-matrix composite. *Acta Metall Mater* 1990; 38: 185-94.
- [134] Lee BJ, Mear ME. Effect of inclusion shape on stiffness of isotropic and transversely isotropic two-phase composites. *Int J Solids Struct* 1991; 28: 975-1001.
- [135] Lee BJ, Mear ME. Effect of inclusion shape on stiffness of nonlinear two-phase composites. *J Mech Phys Solids* 1991; 39: 627-49.
- [136] Banks-Sills L, Leiderman V, Fang D. On the effect of particle shape and orientation on elastic properties of metal matrix composites. *Composites: Part B* 1997; 28B:465-81.
- [137] Iijima S. Helical microtubes of graphitic carbon. *Nature* 1991; 354: 56-8.
- [138] Treacy MMJ, Ebbesen TW, Gibson TM. Exceptionally high Young's modulus observed for individual carbon nanotubes. *Nature* 1996; 381: 680-7.
- [139] Popov VN, Van Doren EV, Balkanski M. Elastic properties of single-walled carbon nanotubes. *Phys Rev B* 2000; 61: 3078-84.
- [140] Uddin MF, Sun CT. Strength of unidirectional glass/epoxy composite with silica nanoparticle-enhanced matrix. *Compos Sci Technol* 2008; 68: 1637-43.

- [141] Zhang J, Wu T, Wang L, Jiang W, Chen L. Microstructure and properties of  $Ti_3SiC_2/SiC$  nanocomposites fabricated by spark plasma sintering. *Compos Sci Technol* 2008; 68: 499-505.
- [142] Tsai JL, Wu MD. Organoclay effect on mechanical responses of glass/epoxy nanocomposites. *J Compos Mater* 2007; 41: 2513.
- [143] Cho J, Chen JY, Daniel IM. Mechanical enhancement of carbon fiber/epoxy composites by graphite nanoplatelet reinforcement. *Scripta Mater* 2007; 56: 685.
- [144] Kanagaraj S, Varanda FR, Zhiltsova TV, Oliveira MSA, Simoes JAO. Mechanical properties of high density polyethylene/carbon nanotube composites. *Compos Sci Technol* 2007; 67: 3071-7.
- [145] Katti KS, Sikdar D, Katti DR, Ghosh P, Verma D. Molecular interactions in intercalated organically modified clay and clay-polycaprolactam nanocomposites: experiments and modeling. *Polymer* 2006; 47: 403-14.
- [146] Wang ZD, Lu JJ, Li Y, Fu SY, Jiang SQ, Zhao XX. Studies on thermal and mechanical properties of  $PI/SiO_2$  nanocomposite films at low temperature. *Composite A* 2006; 37: 74-9.
- [147] Buryachenko VA, Roy A, Lafdi K, Anderson KL, Chellapilla S. Multi-scale mechanics of nanocomposites including interface: experimental and numerical investigation. *Compos Sci Technol* 2005; 65: 2435-65.
- [148] Dalton BA, Collins S, Munoz E, Razal MJ, Von Howaed E, Ferraris PJ, et al. Super-tough carbon-nanotube fibers. *Nature* 2003; 423: 703-5.
- [149] Zhu HW, Xu CL, Wu DH, Wei BQ, Vajtai R, Ajayan PM. Direct synthesis of long single-walled carbon nanotube strands. *Science* 2002; 296: 884-6.
- [150] Yu MF, Lourie O, Dyer MJ, Moloni K, Kelly TF, Ruoff RS. Strength and breaking mechanics of multiwalled carbon nanotubes under tensile load. *Science* 2000; 287: 637-40.
- [151] Li F, Cheng HM, Bai S, Su G, Dresselhaus MS. Tensile strength of single-walled carbon nanotubes directly measured from their macroscopic ropes. *Appl Phys Lett* 2000; 77: 3161-3.
- [152] Bower C, Rosen R, Jin L, Han J, et al. Deformation of carbon nanotubes in nanotube-polymer composites. *Appl Phys Lett* 1999; 74: 3317-19.
- [153] Schadler LS, Giannaris SC, Ajayan PM. Load transfer in carbon nanotube epoxy composites. *Appl Phys Lett* 1998; 73: 3842-44.
- [154] Wagner HD, Lourie O, Feldman Y, Tenne R. Stress-induced fragmentation of multiwall carbon nanotubes in a polymer matrix. *Appl Phys Lett* 1998; 72: 188-90.
- [155] Wong EW, Sheehan PE, Lieber CM. Nanobeam mechanics: elasticity, strength, and toughness of nanorods and nanotubes. *Science* 1997; 277: 1971-5.
- [156] Boutaleb S, Zairi F, Mesbah A, Nait-Abdelaziz M, Gloaguen JM, Boukharouba T, Lefebvre JM. Micromechanics-based modeling of stiffness and yield stress for silica/polymer nanocomposites. *Int J Solids Struct* 2009; 46: 1716-26.

- [157] Ashrafi B, Hubert P. Modeling the elastic properties of carbon nanotube array/polymer composites. *Compos Sci Technol* 2006; 66: 387-96.
- [158] Berhan L, Yi YB, Sastry AM, Munoz E, Selvidge M, Baughman RJ. Mechanical properties of nanotube sheets: Alterations in joint morphology and achievable moduli in manufacturable materials. *Appl Phys* 2004; 95: 4335-45.
- [159] Odegard GM, Pipes RB, Hubert P. Comparison of two models of SWCN polymer composites. *Comp Sci Technol* 2004; 64: 1011-20.
- [160] Thostenson ET, Chou TW. On the elastic properties of carbon nanotube-based composites: modeling and characterization. *J Appl Phys D* 2003; 36: 573-82.
- [161] Pipes RB, Hubert P. Scale effects in carbon nanostructures: self-similar analysis. *Nano Lett* 2003; 3: 239-43.
- [162] Pipes RB, Hubert P. Helical carbon nanotube arrays: mechanical properties. *Compos Sci Technol* 2002; 62: 419-28.
- [163] Tu ZC, Ou-yang ZC. Single-walled and multiwalled carbon nanotubes viewed as elastic tubes with the effective Young's moduli dependent on layer number. *Phys Rev B* 2002; 65: 233-407.
- [164] Zhou G, Duan WH, Gu BL. First-principles study on morphology and mechanical properties of single-walled carbon nanotube. *Chem Phys Lett* 2001; 333: 344-9.
- [165] Qian D, Liu WK, Ruoff RS. Mechanics of  $C_{60}$  in nanotubes. *J Phys Chem B* 2001; 105: 10753-8.
- [166] Govindjee S, Sackman JL. On the use of continuum mechanics to estimate the properties of nanotubes. *Solid State Comm* 1999; 110: 227-30.
- [167] Gao GH, Cagin T, Goddard WA. Energetics, structure, mechanical and vibrational properties of single-walled carbon nanotubes. *Nanotech* 1998; 9: 184-91.
- [168] Krishnan A, Dujardin E, Ebbesen TW, Yianilos PN, Treacy MMJ. Young's modulus of single-walled nanotubes. *Phys Rev B* 1998; 58: 14013-9.
- [169] Cornwell CF, Wille LT. Elastic properties of single-walled carbon nanotubes in compression. *Solid State Comm* 1997; 101: 555-8.
- [170] Lee WJ, Son JH, Kang NH, Park IM, Park YH. Finite-element analysis of deformation behaviors in random-whisker-reinforced composite. *Scripta Mater* 2009; 61: 580-3.
- [171] Qiao R, Brinson C. Simulation of interphase percolation and gradients in polymer nanocomposites. *Compos Sci Technol* 2009; 69: 491-9.
- [172] Tserpes KI, Papanikos P, Labeas G, Pantelakis SpG. Multi-scale modeling of tensile behavior of carbon nanotube-reinforced composites. *Theoret Appl Fract Mech* 2008; 49: 51-60.
- [173] Gonzalez C, Llorca J. Mechanical behavior of unidirectional fiber-reinforced polymers under transverse compression: microscopic mechanisms and modeling. *Compos Sci Technol* 2007; 67: 2795-806.
- [174] Saber-Samandari S, Afaghi-Khatibi A. Evaluation of elastic modulus of polymer matrix nanocomposites. *Polym Compos* 2007; 28: 405-11.

- [175] Scocchi G, Posocco P, Fermeglia M, Pricl S. Polymer–clay nanocomposites: a multiscale molecular modeling approach. *J Phys Chem B* 2007;111:2143–51.
- [176] Fermeglia M, Pricl S. Multiscale modeling for polymer systems of industrial interest. *Prog Org Coat* 2007;58:187–99.
- [177] Hbaieb K, Wang QX, Chia YHJ, Cotterell B. Modeling stiffness of polymer/clay nanocomposites. *Polymer* 2007; 48: 901-9.
- [178] Chawla N, Sidhu RS, Ganesh VV. Three-dimensional visualization and microstructure-based modeling of deformation in particle-reinforced composites. *Acta Mater* 2006; 54: 1541-8.
- [179] Cannillo V, Bondioli F, Lusvardi L, Montorsi M, Avella M, Errico ME, Malinconico M. Modeling of ceramic particles filled polymer-matrix nanocomposites. *Compos Sci Technol* 2006; 66: 1031-7.
- [180] Li C, Chou TW. Multiscale modeling of compressive behavior of carbon nanotube/polymer composites. *Compos Sci Technol* 2006; 66: 2409-14.
- [181] Ji B, Gao H. Elastic properties of nanocomposite structure of bone. *Compos Sci Technol* 2006; 66: 1212-8.
- [182] Bondioli F, Cannillo V, Fabbri E, Messori M. Epoxy-silica nanocomposites: preparation, experimental characterization, and modeling. *J Appl Polym Sci* 2005; 97: 2382-2386.
- [183] Borodin O, Bedrov D, Smith GD, Nairn J, Bardenhagen S. Multiscale modeling of viscoelastic properties of polymer nanocomposites. *J Polym Sci Part B: Polym Phys* 2005; 43:1005–13.
- [184] Buryachenko VA. Effective elastic moduli of triply periodic particulate matrix composites with imperfect unit cells. *Int J Solids Struct* 2005;42:4811–32.
- [185] Shi D, Feng X, Jiang H, Huang YY, Hwang K. Multiscale analysis of fracture of carbon nanotubes embedded in composites. *Int J Fract* 2005; 134: 369–86.
- [186] Buryachenko VA, Tandon GP. Estimation of effective elastic properties of random structure composites for arbitrary inclusion shape and anisotropy of components using finite element analysis. *Int J Multiscale Comput Engng* 2004;2:29–45.
- [187] Avella M, Bondioli F, Cannillo V, Errico ME, Ferrari AM, Focher B. Preparation, characterisation and computational study of poly (epsilon-caprolactone) based nanocomposites. *Mater Sci Technol* 2004;20:1340–4.
- [188] Chen XL, Liu YJ. Square representative volume elements for evaluating the effective material properties of carbon nanotube-based composites. *Comput Mater Sci* 2004; 29: 1-11.
- [189] Sheng N, Boyce MC, Parks DM, Rutledge GC, Abes JI, Cohen RE. Multiscale micromechanical modeling of polymer nanocomposites and the effective clay particle. *Polymer* 2004; 45:487–506.
- [190] Porter D. Pragmatic multiscale modelling of bone as a natural hybrid nanocomposite. *Mater Sci Eng A* 2004; 365:38–45.

- [191] Fisher FT, Bradshaw RD, Brinson LC. Fiber waviness in nanotube-reinforced polymer composites-I: modulus predictions using effective nanotube properties. *Compos Sci Technol* 2003;63:1689–703.
- [192] Bradshaw RD, Fisher FT, Brinson LC. Fiber waviness in nanotube-reinforced polymer composites-II: modeling via numerical approximation of the dilute strain concentration tensor. *Compos Sci Technol* 2003;63:1705–22.
- [193] Li C, Chou TW. A structural mechanics approach for the analysis of carbon nanotubes. *Int J Solids Struct* 2003;40:2487–99.
- [194] Liu YJ, Chen XL. Evaluations of the materials properties of carbon nanotube-based composites using a nanoscale representative volume element. *Mech Mater* 2003; 35: 69-81.
- [195] Odegard GM, Gates TS, Nicholson LM, Wise KE. Equivalent continuum modeling of nano-structured materials. *Compos Sci Technol* 2002;62:1869–80.
- [196] Starr FW, Glotzer SC. Simulations of filled polymers on multiple length scales. In: Nakatani AI, Hjelm RP, Gerspacher M, Krishnamoorti R, editors. *Filled and Nanocomposite Polymer Materials, Materials Research Symposium Proceedings*. Warrendale: Materials Research Society, 2001. pp. KK4.1.1–KK4.1.13.
- [197] Glotzer SC, Starr FW. Towards multiscale simulations of filled and nanofilled polymers. In: Cummings PT, Westmoreland PR, Carnahan B, editors. *Foundations of Molecular Modeling and Simulation: Proceedings of the 1st international conference on molecular modeling and simulation*. Keystone: American Institute of Chemical Engineers, 2001. pp. 44–53.
- [198] Ogata S, Lidorikis E, Shimojo F, Nakano A, Vashishta P, Kalia RK. Hybrid finite-element/molecular-dynamics/electronic-density-functional approach to materials simulations on parallel computers. *Comp Phys Comm* 2001; 138: 143-54.
- [199] Hyer MW. *Stress analysis of fiber-reinforced composite materials*. McGraw-Hill, Boston, 1998.
- [200] Nemat-Nasser S, Hori M. *Micromechanics: Overall properties of heterogeneous materials*. Elsevier, Amsterdam, 1999.
- [201] Zhang P, Huang Y, Geubelle PH, Klein PA, Hwang KC. The elastic modulus of single-wall carbon nanotubes: a continuum analysis incorporating interatomic potential. *Int J Solids Struct* 2002;39: 3893–906.
- [202] Tserpes KI, Papanikos P. A progressive fracture model for carbon nanotubes. *Compos Part B* 2006; 37: 662-9.
- [203] Belytschko T, Xiao S, Schatz G, Ruoff R. Atomistic simulations of nanotube fracture. *Phys Rev B* 2002; 65: 235430.
- [204] Steglich D, Siegmund T, Brocks W. Micromechanical modeling of damage due to particle cracking in reinforced metals. *Comput Mater Sci* 1999; 16: 404-13.
- [205] Langer SA, Fuller ER, Carter WC. OOF: an image-based finite element analysis of material microstructures. *Comput Sci Eng* 2001;3:15–23.

- [206] Langer SA, Reid ACE, Haan SI, Garcia RE. The OOF2 manual: Revision 3.2 for OOF2 Version 2.0 beta 8, NIST, USA. Online: <http://www.ctcms.nist.gov/~langer/oof2man/index.html>.
- [207] Ganesh VV, Chawla N. Effect of particle orientation anisotropy on the tensile behavior of metal matrix composites: experiments and microstructure-based simulation. *Mater Sci Eng A* 2005; 391: 342-53.
- [208] Cannillo V, Manfredini T, Montorsi M, Boccaccini AR. Use of numerical approaches to predict mechanical properties of brittle bodies containing controlled porosity. *J Mater Sci* 2004;39:4335–7.
- [209] Cannillo V, Manfredini T, Montorsi M, Boccaccini AR. Investigation of the mechanical properties of Mo-reinforced glassmatrix composites. *J Non-Crystal Solids* 2004;344:88–93.
- [210] Chawla N, Patel BV, Kopman M, Chawla KK, Saha R, Patterson BR, Fuller ER, Langer SA. Microstructure-based simulation of thermomechanical behavior of composite materials by object-oriented finite element analysis. *Mater Characteriz* 2003; 49: 395–407.
- [211] Cannillo V, Pellacani GC, Leonelli C, Boccaccini AR. Numerical modeling of the fracture behavior of a glass matrix composite reinforced with alumina platelets. *Composites Part A* 2003;34:43–51.
- [212] Cannillo V, Leonelli C, Manfredini T, Montorsi M, Boccaccini AR. Computational simulations for the assessment of the mechanical properties of glass with controlled porosity. *J Porous Mater* 2003;10:189–200.
- [213] Wang Z, Kulkarni A, Deshpande S, Nakamura T, Herman H. Effects of pores and interfaces on effective properties of plasma sprayed zirconia coatings. *Acta Mater* 2003; 51: 5319-34.
- [214] Zimmermann MH, Baskin DM, Faber KT, Fuller Jr ER, Allen AJ, Keane DT. Fracture of a textured anisotropic ceramic. *Acta Mater* 2001;49:3231–42.
- [215] Zimmermann A, Carter WC, Fuller ER. Damage evolution during microcracking of brittle solids. *Acta Mater* 2001;49:127–37.
- [216] Saigal A, Fuller Jr ER, Langer SA, Carter WC, Zimmermann MH, Faber KT. Effect of interface properties on microcracking of iron titanate. *Scripta Mater* 1998;38:1449–53.
- [217] Avella M, Bondioli F, Cannillo V, Errico ME, Ferrari AM, Focher B, Malinconico M, Manfredini T, Montorsi M. Preparation, characterization and computational study of poly ( $\epsilon$ -caprolactone) based nanocomposites. *Mater Sci Technol* 2004;20:1340–4.
- [218] Iwahori Y, Ishiwata S, Sumizawa T, Ishikawa T. Mechanical properties improvements in two-phase and three-phase composites using carbon nanofiber dispersed resin. *Compos Part A* 2005; 36: 1430.
- [219] Wang H, Bai Y, Liu S, Wu J, Wong CP. Combined effects of silica filler and its interface in epoxy resin. *Acta Mater* 2002; 50: 4369-77.
- [220] Lan T, Pinnavaia TJ. Clay-reinforced nanocomposites. *Chem Mater* 1994; 6: 2216-9.
- [221] Subramaniyan AK, Sun CT. Enhancing compressive strength of unidirectional polymeric composites using nanoclay. *Compos Part A* 2006; 37: 2257.

- [222] Wetzel B, Hauptert F, Zhang MQ. Epoxy nanocomposites with high mechanical and tribological performance. *Compos Sci Technol* 2003; 63: 2055-67.
- [223] Ou Y, Yang F, Yu ZZ. A new conception on the toughness of nylon 6/silica nanocomposite prepared via in situ polymerization. *J Polym Sci B* 1998; 36: 789-95.
- [224] Cho J, Joshi MS, Sun CT. Effect of inclusion size on mechanical properties of polymeric composites with micro and nanoparticles. *Compos Sci Technol* 2006; 66: 1941-52.
- [225] Chisolm N, Mahfuz H, Rangari VK, Adnan A, Jeelani S. Fabrication and mechanical characterization of carbon/SiC-epoxy nanocomposites. *Compos Struct* 2005; 67: 115-24.
- [226] Voros G, Pukanszky B. Prediction of the yield stress of composites containing particles with an interlayer of changing properties. *Composites A* 2002; 33: 1317-22.
- [227] Reynaud E, Jouen T, Gauthier C, Vigier G, Varlet J. Nanofillers in polymeric matrix: a study on silica reinforced PA6. *Polymer* 2001; 42: 8759-68.
- [228] Kontou E, Anthoulis G. The effect of silica nanoparticles on the thermomechanical properties of polystyrene. *J Appl Polym Sci* 2007; 105: 1723-31.
- [229] Saber-Samandari S, Khatibi AA. The effect of interphase on the elastic modulus of polymer based nanocomposites. In: Liu HY, Hu XZ, Hoffman M, editors. *Fracture of materials: moving forwards*. Switzerland: Tans Tech Publications; 2006. pp. 199–204.
- [230] Carrado KA, Xu L. In situ synthesis of polymer-clay nanocomposites from silicate gels. *Chem Mater* 1998; 10: 1440-5.
- [231] Schiotz J, Jacobsen KW. A maximum in the strength of nanocrystalline copper. *Science* 2003; 301: 1357-59.
- [232] Chen Q, Chasiotis I, Chen C, Roy A. Nanoscale and effective mechanical behavior and fracture of silica nanocomposites. *Compos Sci Technol* 2008; 68: 3137-44.
- [233] Adachi T, Osaki M, Araki W, Kwon S. Fracture toughness of nano- and micro-spherical silica-particle-filled epoxy composites. *Acta Mater* 2008; 56: 2101-9.
- [234] Zhang H, Zhang Z, Friedrich K, Eger C. Property improvements of in situ epoxy nanocomposites with reduced interparticle distance at high nanosilica content. *Acta Mater* 2006; 54: 1833.
- [235] Ragosta G, Abbate M, Musto P, Scarinzi G, Mascia L. Epoxy-silica particulate nanocomposites: chemical interactions, reinforcement and fracture toughness. *Polymer* 2005; 46: 10506.
- [236] Choi S, Awaji H. Nanocomposites-a new material design concept. *Sci Technol Adv Mater* 2005; 6: 2-10.
- [237] Lee J, Yee AF. Fracture of glass bead/epoxy composites: on micro-mechanical deformations. *Polymer* 2000; 41: 8363.
- [238] Gao L, Wang HZ, Hong JS, Miyamoto H, Miyamoto K, Nishikawa Y, de la Torre D. Mechanical properties and microstructures of nano-SiC-Ai<sub>2</sub>O<sub>3</sub> composites densified by spark plasma sintering. *J Eur Ceram Soc* 1999; 19: 609-13.

- [239] Davidge RW, Brook RJ, Cambier F, Poorteman M, Leriche A, O'sullivan D, Hampshire S, Kennedy T. Fabrication, properties, and modeling of engineering ceramics reinforced with nanoparticles of silicon carbide. *Br Ceram Trans* 1997; 96: 121-7.
- [240] Carroll L, Sternitzke M, Derby B. Silicon Carbide particle size effects in alumina-based nanocomposites. *Acta Mater* 1996; 44: 4543-52.
- [241] Zhao J, Steans LC, Harmer MP, Chan HM, Miller GA, Cook RF. Mechanical behavior of alumina-silicon carbide nanocomposites. *J Am Ceram Soc* 1993; 76: 503-10.
- [242] Niihara K. New design concept of structural ceramics-ceramic nanocomposites. *J Ceram Soc Japan* 1991; 99: 974-82.
- [243] Awaji H, Choi SM. Review: ceramic-based nanocomposites. In: SG Pandalai (Ed.), *Recent Research Developments in Materials Science & Engineering* 2002; 1: 585-597.
- [244] Awaji H, Choi SM, Yagi E. Mechanisms of toughening and strengthening in ceramic-based nanocomposites. *Mech Mater* 2002; 34: 411-22.
- [245] Xiao SP, Belytschko T. A bridge domain method for coupling continua with molecular dynamics. *Comput Methods Appl Mech Eng* 2004; 193: 1645-69.